Technical Report
**TR-17-16**
July 2018

# Stress corrosion testing of copper in sulfide solutions

Claes Taxén
Jesper Flyg
Hans Bergqvist

SVENSK KÄRNBRÄNSLEHANTERING AB

SWEDISH NUCLEAR FUEL
AND WASTE MANAGEMENT CO

Box 3091, SE-169 03 Solna
Phone +46 8 459 84 00
skb.se

SVENSK KÄRNBRÄNSLEHANTERING

ISSN 1404-0344
**SKB TR-17-16**
ID 1614013

July 2018
Updated 2019-10

# Stress corrosion testing of copper in sulfide solutions

Claes Taxén, Jesper Flyg, Hans Bergqvist
Swerea KIMAB AB

The original report, dated July 2018, was found to contain editorial errors which have been corrected in this updated version.

# Summary

Copper rods were tested for signs of stress corrosion cracking in artificial sea water with and without addition of 10 mM sulfide. Tests were performed by slow strain rate testing at ambient temperature and at 80 °C. Two types of test rods were used. Rods with round cross sections had a diameter of 7 mm. Rods with rectangular cross section had the dimensions of $2 \times 4$ mm at the narrow section. The extension rate was $10^{-6}$ $s^{-1}$ until fracture.

Stress-strain curves show no signs of stress corrosion cracking. Addition of 10 mM sulfide caused no significant difference in the curves. Examination of the specimens by microscopy and by SEM also showed no signs of stress corrosion cracking. However, superficial intergranular corrosion was observed at some sites for rods tested at 80 °C. Similar corrosion patterns have by other researchers been interpreted as signs of stress corrosion cracking. The results are discussed in relation to previous work with the aim of identifying differences in experimental conditions that could explain apparent differences in the tendency for stress corrosion cracking in sulfidic solutions.

# Contents

# 1 Introduction

## 1.1 General

Copper is the canister material selected for final disposal of spent nuclear fuel in the Swedish concept. Stress Corrosion Cracking (SCC) is one mode of failure that is being investigated. The assessment of SCC for the post-closure safety is described in the fuel and canister process report (SKB 2010), with supporting details in King and Newman (2010). It was concluded that the probability of SCC under the early aerobic phase is low due to the absence of the necessary conditions, and that there is no well-founded mechanism for cracking during the anaerobic phase.

There was though one published study on stress corrosion that indicates that copper could be sensitive to SCC in solutions containing sulfide (Taniguchi and Kawasaki 2008). Efforts to corroborate these findings have since been made but no signs of SCC have been found in these studies (Bhaskaran et al. 2013, Sipilä et al. 2014).

The present work aims at determining whether copper is sensitive to SCC under conditions similar to those studied by Taniguchi and Kawasaki. The first set of tests uses in house best practice for SCC using Slow Strain Rate Testing (SSRT). This practice uses test rods with circular cross section and annealed material. Taniguchi and Kawasaki used test rods with rectangular cross section and a material that probably was not annealed. The second set of test uses test rods made from the drawings published by Taniguchi and Kawasaki and material that was not fully annealed so that various degrees of cold work remained from rolling.

Parallel to our work, the Swedish Radiation Safety Authority (SSM) carried out studies of SCC of copper in sulfide solutions at Studsvik (Becker and Öijerholm 2017). For tests at 90 °C, they found features that they interpreted as signs of SCC.

In view of the apparent discrepancies in the results of Taniguchi and Kawasaki (Taniguchi and Kawasaki 2008) and Becker and Öijerholm (Becker and Öijerholm 2017) on one hand and the results of Bhaskaran et al. (Bhaskaran et al. 2013) on the other hand, a rather detailed account the experimental conditions and the results is given in this chapter.

## 1.2 The work of Taniguchi and Kawasaki 2008

### 1.2.1 Experimental details

Material: Phosphorous–deoxidised copper used in trial manufacture of copper overpack was selected as the coupon material. The chemical impurities in the copper are shown in Table 2-1.

Pretreatment: The coupon surfaces were polished with 3 μm, micro grit diamond paste prior to the SSRT. Geometry of coupons for slow strain rate test, rectangular 4 × 2 mm, see Figure 1-1.

Test temperature: 353 K (80 °C).

Extension rate: $8.3 \times 10^{-7}$ $s^{-1}$.

The test solutions in the cell were renewed every few days with 3 days maximum interval.

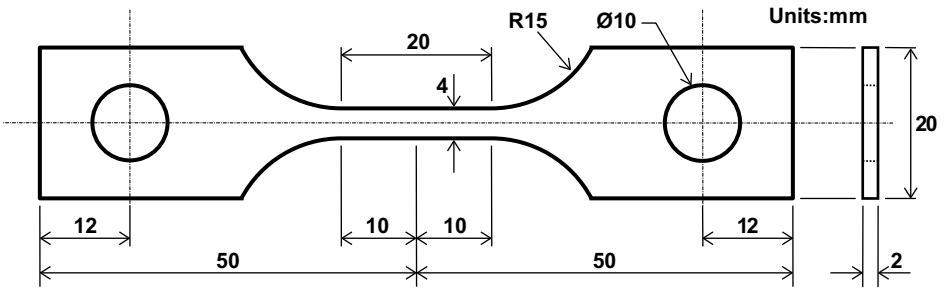


***Figure 1-1.*** *Geometry of coupons for the slow strain rate tests. (Taniguchi and Kawasaki 2008.)*

The electrode potential was fixed at the rest potential value in an $N_2$ atmosphere measured under the same conditions in advance of the SSRT. The rest potentials in synthetic seawater containing $Na_2S$ are shown in Table 1-1.

**Table 1-1. Rest potentials for copper in synthetic seawater with various concentrations of sulfide.**

| Rest potential for copper in synthetic seawater (mV vs. SCE) | Sulfide Concentration (M) |
|---|---|
| −450 | 0 |
| −880 | 0.001 |
| −920 | 0.005 |
| −950 | 0.010 |

The composition of the copper material tested will be shown in Section 2.2 for comparison with materials used in other studies.

Table 1-2 shows the composition and pH of the synthetic seawater used.

**Table 1-2. Composition and pH of synthetic seawater (Taniguchi and Kawasaki 2008).**

| Component | Concentration (M) |
|---|---|
| $Cl^-$ | 0.56 |
| $SO_4^{2-}$ | 0.029 |
| $HCO_3^-$ | 0.0024 |
| $F^-$ | 0.000074 |
| $Br^-$ | 0.00086 |
| $BO_3^-$ | 0.00044 |
| $Na^+$ | 0.48 |
| $K^+$ | 0.010 |
| $Ca^{2+}$ | 0.010 |
| $Mg^{2+}$ | 0.055 |
| $Sr^{2+}$ | 0.00070 |
| pH | 7.9–8.4 |

### 1.2.2 Results

Figure 1-2 shows the influence of sulfide concentration on the stress–strain curve of the copper tested.

Figure 1-2 shows that the elongation at failure is the same in synthetic seawater as in silicon oil. The concentration 0.001 M sulfide in the seawater would seem to have a positive effect whereas 0.005 M sulfide gives the same elongation at fracture as pure synthetic seawater and 0.01 M sulfide gives a slightly lower elongation at fracture.

Figure 1-3 shows SEM microphotographs of coupon surfaces after SSRT test. Figure 1-4 shows cross sectional observations of the copper coupons after test in various sulfide-containing solutions.

Quoted from the publication by Taniguchi and Kawasaki (with the figure number in [ ] referring to the present report):

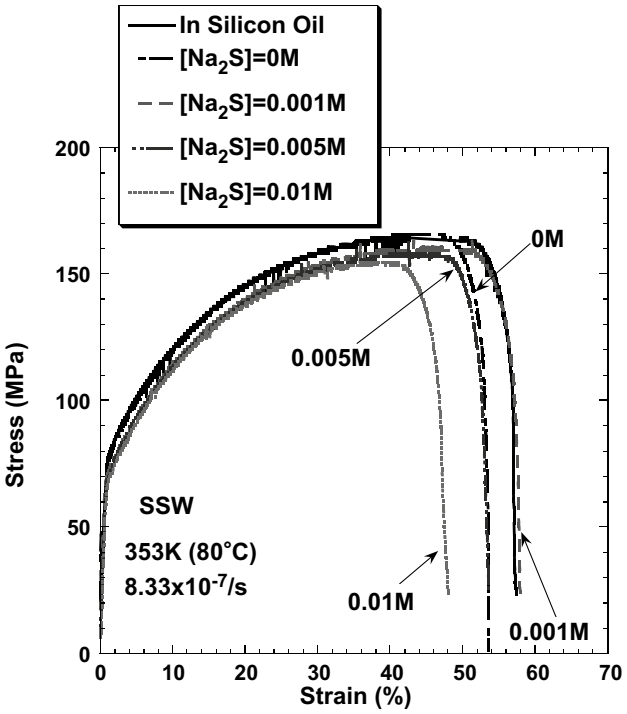


***Figure 1-2.*** *Influence of sulfide concentration on the stress–strain curve of pure copper (Taniguchi and Kawasaki 2008).*

"The stress-strain curves obtained by SSRT are shown in [Figure 1-2]. The influence of sulfide on the curve was not definitive up to 0.005 M, whereas distinct decrease of maximum stress and strain to failure was observed at the higher sulfide concentration of 0.01 M. [Figure 1-3] shows the SEM photomicrographs of coupon surfaces near the fractured location after the SSRT. No cracks or selective metal dissolution were found on the coupon surfaces in the tests in silicone oil and in 0.0 M-$Na_2S$ solution. This result shows that crack or local attack is not likely to be initiated on the coupon surface in inert environment and in sulfide free environment during SSRT. In sulfide environment, copper coupons were attacked by selective dissolution or SCC. For 0.001 M-$Na_2S$, a few narrow slits were observed near the fractured location and seemed to be along slip lines or grain boundaries, but were not able to be classified into neither SCC nor selective dissolution. At the higher $Na_2S$ concentration of 0.005 M, some crevasses suspected to be SCC were observed near the fractured location. In the case of the much higher $Na_2S$ concentration of 0.01 M, numerous, obvious cracks were observed over the coupon surface. [Figure 1-4] shows the results of cross sectional observations near the fractured location where indications of cracking or selective dissolution were observed. In the case of 0.001 M solutions, although the initiations of micro cracks were indicated on the surface, it seems to have propagated as intergranular corrosion rather than SCC. As for 0.005 M, concave pitting was observed and it was not likely SCC but a kind of selective dissolution. Typical SCC was observed in the tests in 0.01 M solutions and seems to have propagated along grain boundaries, therefore, the SCC mode for phosphorous–deoxidised copper in a sulfide environment is assumed to be an intergranular type. From the cross sectional observations, the slits or crevasses observed by SEM for 0.001 M and 0.005 M solutions were not attributable to SCC. Such an interpretation agreed with the stress-strain curve behavior such that obvious reduction in ductility did not appear up to 0.005 M.

It can be summarised that copper is susceptible to intergranular attack by sulfide such as selective dissolution at lower sulfide concentration and SCC at higher sulfide concentration. The threshold of sulfide concentration for SCC initiation is likely to be in the range of 0.005–0.01 M under our experimental condition."

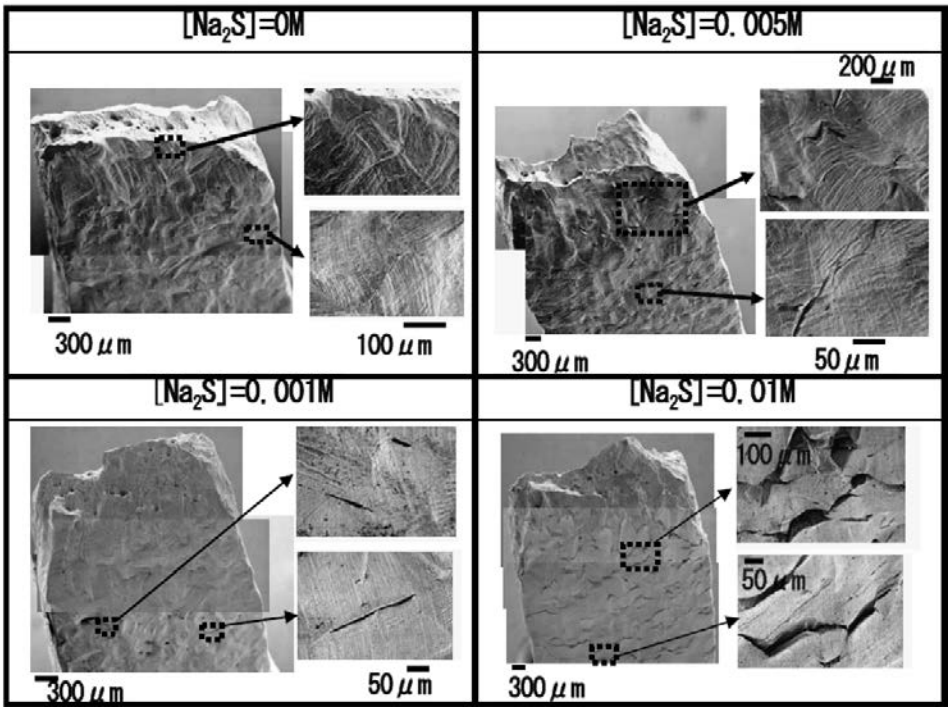


***Figure 1-3.*** *SEM microphotographs of coupon surfaces after SSRT tests (Taniguchi and Kawasaki 2008).*

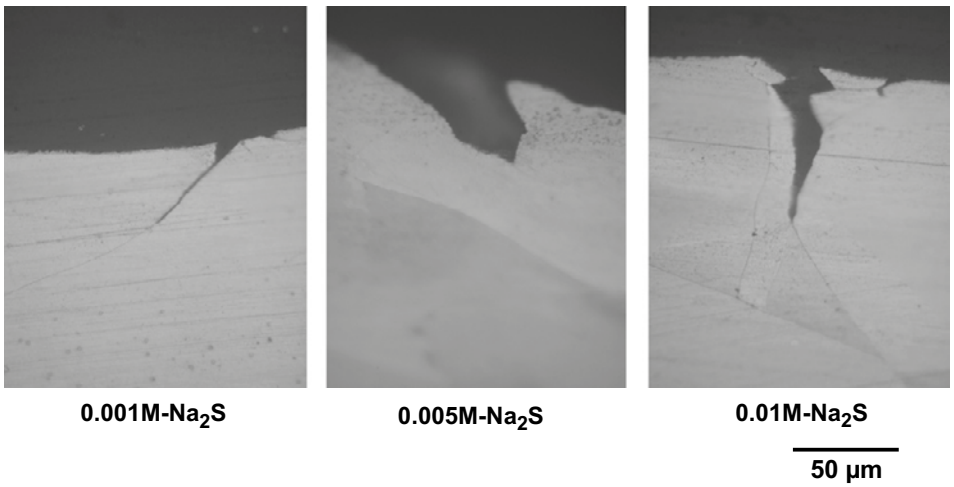


***Figure 1-4.*** *Results of cross sectional observation of copper coupon after SSRT tests (Taniguchi and Kawasaki 2008).*

## 1.3 The work of Bhaskaran et al. 2013

### 1.3.1 Experimental details

Bhaskaran et al. (Bhaskaran et al. 2013) used copper tensile specimens from Cu-OFP provided by SKB. Specimens were taken from the lid center, the lid edge or the container wall.

The geometry of the test objects is shown in Figure 1-5.

The gauge length part of each tensile specimen was etched for 2–3 minutes at 1.2 V after electro-polishing in 57 wt.% phosphoric acid for 5–10 minutes at 1.8 V versus a copper cathode. In some tests, that part of the surface was just abraded with silicon carbide paper to a 1 200 grit finish.

Table 1-3 shows the nominal composition of the synthetic seawater supplied by the sea salt provider.

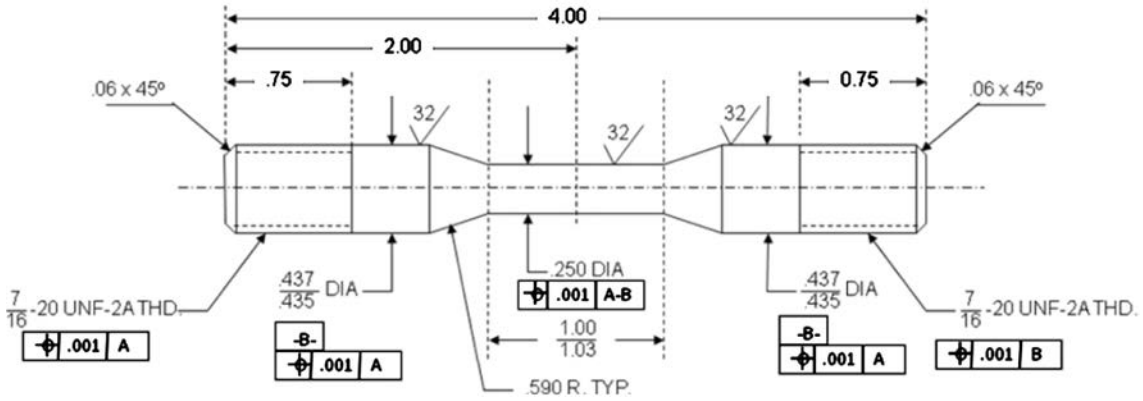


***Figure 1-5.*** *Schematic illustration of the copper SSRT specimen (unit: inch). (Bhaskaran et al. 2013.)*

**Table 1-3. Nominal composition of the synthetic seawater supplied by the sea salt provider (Instant Ocean) (Bhaskaran et al. 2013).**

| Elements | Concentration (mM) |
|---|---|
| $Cl^-$ | 524 |
| $Na^+$ | 452 |
| $SO_4^{2-}$ | 27.1 |
| $Mg^{2+}$ | 53.7 |
| $Ca^{2+}$ | 10.2 |
| $K^+$ | 9.7 |
| $HCO_3^-$ | 2.4 |
| $Sr^{2+}$ | 0.14 |
| $CO_3^{2-}$ | 0.17 |
| $Br^-$ | 0.075 |
| $BO_3^-$ | 0.075 |
| $F^-$ | 0.079 |

The tests were mostly performed at the free corrosion potential of the copper test pieces but in some experiments the potential was controlled at various potentials close to the free corrosion potential, in order to be similar to the work of Taniguchi and Kawasaki.

### 1.3.2 Results

Figure 1-6 shows stress-strain curves for room temperature. The elongation at failure is about 61.5 % in air and about 56.8 % in synthetic seawater with 10 mM $Na_2S$. Cathodic polarisation (−20 mV) gives an elongation of about 59.4 %.

Figure 1-7 shows results for 80 °C in synthetic seawater with 10 mM $Na_2S$. The elongation at failure is the smallest at an applied potential of −800 mV (~53.4 %), −900mV gives an intermediate value (~ 55.4 %) and −950 mV gives the largest elongation at failure (~ 56.9 %).

Figure 1-9 shows cross sections of a tensile specimen after test in synthetic seawater with addition of 10 mM $Na_2S$ at room temperature.

Figure 1-8 shows a polarisation curve for copper in 10 mM sulfide at 80 °C. The fixed potentials applied to the test rods for Figure 1-7 are marked in Figure 1-8.

A tensile specimen cross section is shown in Figure 1-9. Typical specimen surface morphology after testing is shown in Figure 1-10 (Bhaskaran et al. 2013). The authors conclude: “There was never any significant difference in elongation between specimens tested in solution and air.” But the authors note that, with reference to Figure 1-9, that there was general corrosion in every test in sulfide solution.

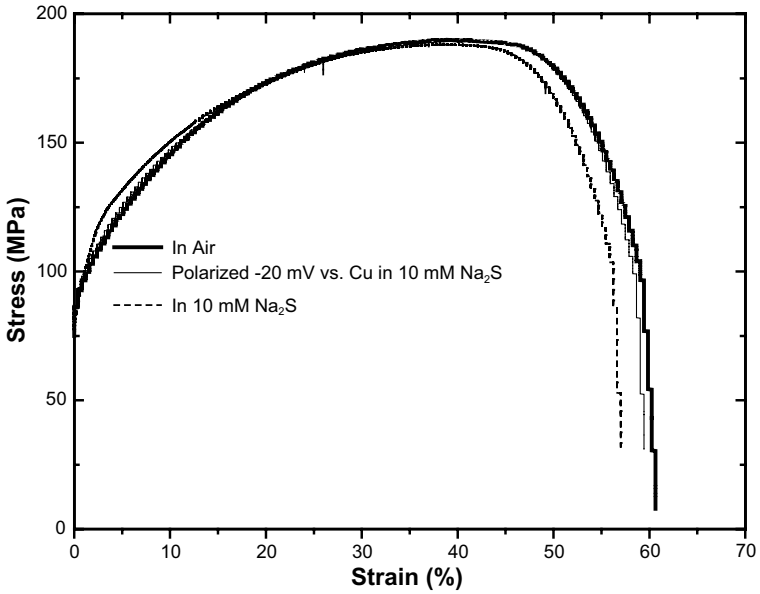


***Figure 1-6.*** *Stress-strain curves obtained at room temperature. One reference curve in air, one curve for a test in synthetic seawater with addition of 10 mM $Na_2S$ and one curve for a test in the same solution where cathodic polarisation was applied. (Bhaskaran et al. 2013.)*

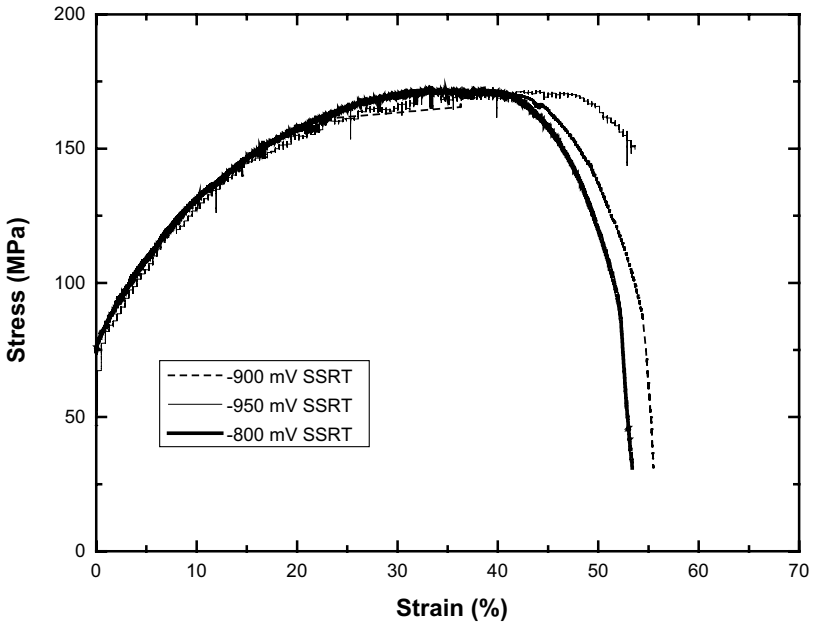


***Figure 1-7.*** *Stress-strain curves obtained at 80 °C. Tests in synthetic seawater with addition of 10 mM $Na_2S$ at various applied potentials. (Bhaskaran et al. 2013.)*

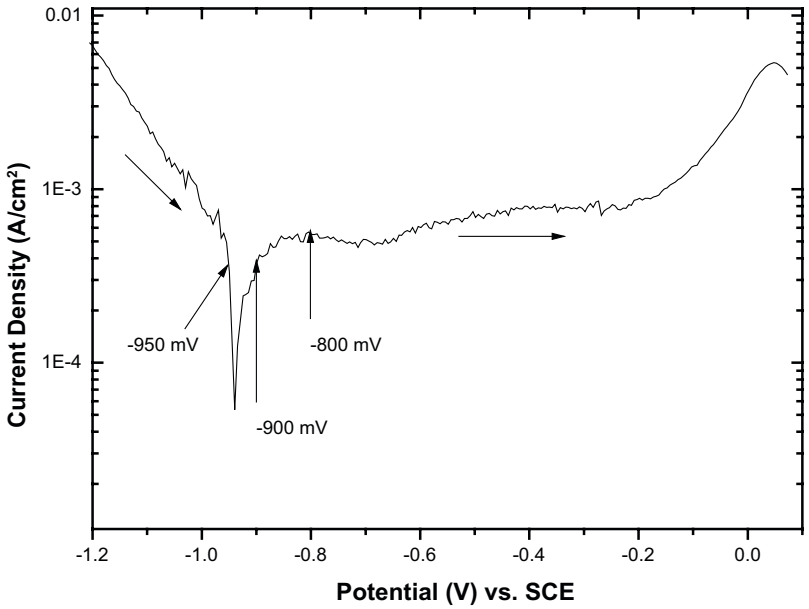


***Figure 1-8.*** *Potentiodynamic scan of copper in synthetic sea water with addition of 10 mM $Na_2S$ at 80 °C. Scan rate was 1 mV/s. (Bhaskaran et al. 2013.)*

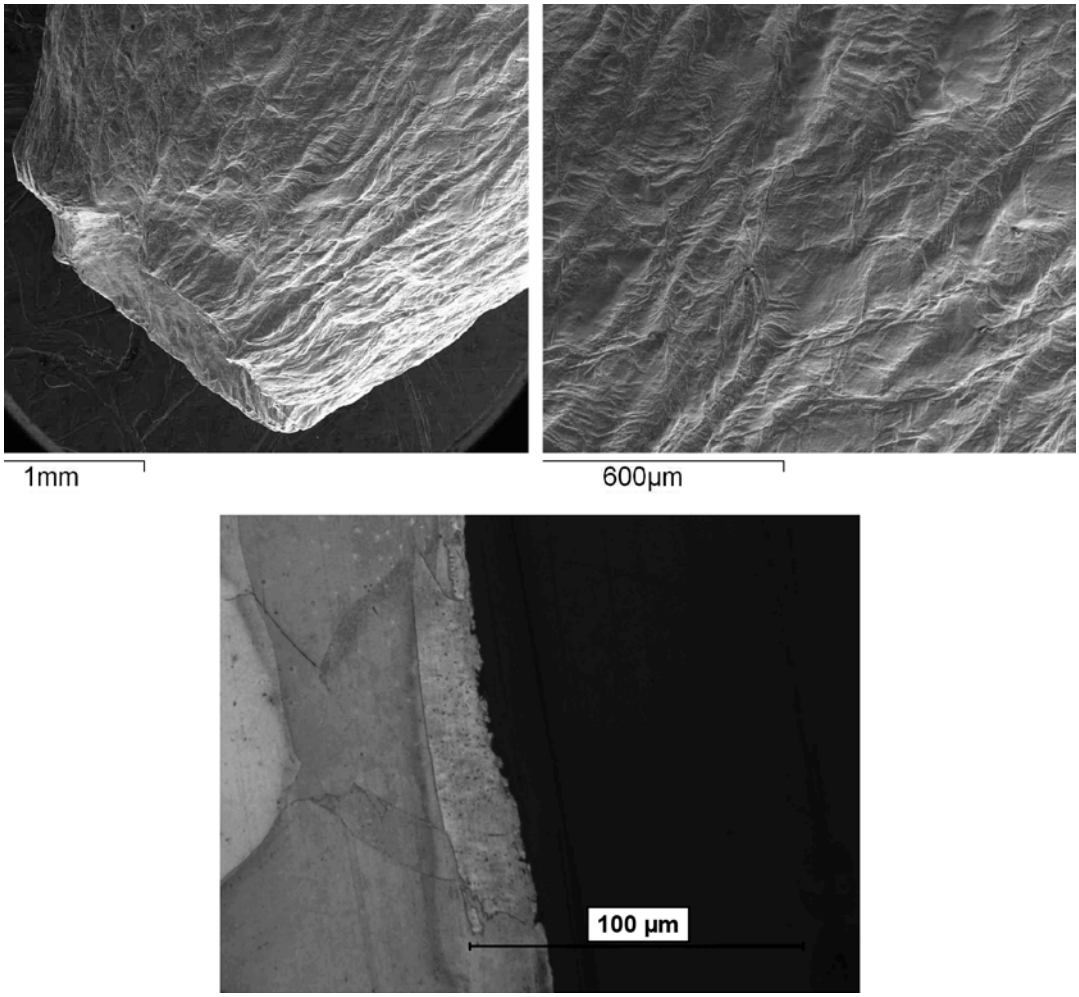


***Figure 1-9.*** *Surface and longitudinal cross section of the tensile specimen tested in synthetic seawater with addition of 10 mM $Na_2S$ at room temperature. (Bhaskaran et al. 2013.)*

One SSRT specimen showed aberrant surface features after test at room temperature in 0.414 M NaCl+1.56 mM $Na_2S$+0.78 mM $Na_2S_2O_3$ (Total of 100 ppm "S"). Figure 1-11 shows what appears to be a granular network on the polished (unetched) cross-sectional surface of this sample. However further examination did not support the notion that this was some kind of deep, penetrating corrosion that had occurred during exposure to the sulfide-thiosulfate solution. Not least, this was because the grain size of the material was much smaller than that of the apparent granular network (Bhaskaran et al. 2013).

One of the few documented observations of grain boundary corrosion comes from the complementary studies and not from the SSRT tests. Figure 1-12 shows the copper surface before (a) and after (b) removal of the corrosion products. The authors conclude: "Wherever there was some indication of intergranularity (e.g.[Figure 1-12]), it turned out to be superficial on closer examination. In any event, there was no evidence of SCC and no evidence of deep, penetrating intergranular corrosion."

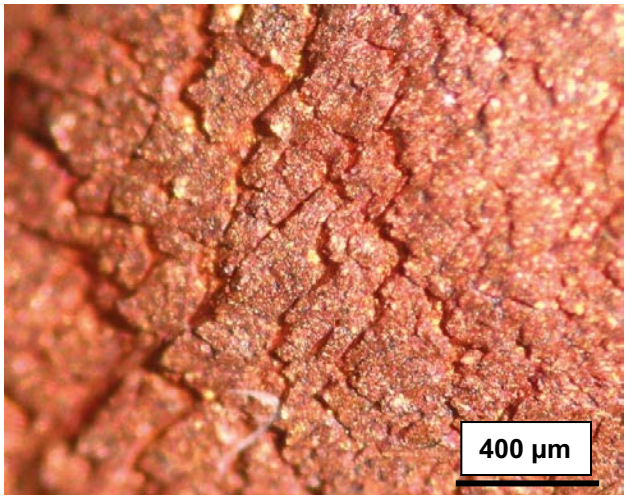


***Figure 1-10.*** *Morphology of the exposed surface of a copper SSRT specimen after removing the sulfide film. 10 mM sulfide in synthetic seawater at 80 °C. The zig-zag patterns are probably due to enhanced corrosion at sites of film fracture. (Bhaskaran et al. 2013.)*

***Figure 1-11.*** *Apparent granular network on a polished, unetched surface of sample exposed in 0.414 M NaCl+1.56 mM $Na_2S$+0.78 mM $Na_2S_2O_3$ at room temperature. The gauge diameter was 3 mm. (Bhaskaran et al. 2013.)*

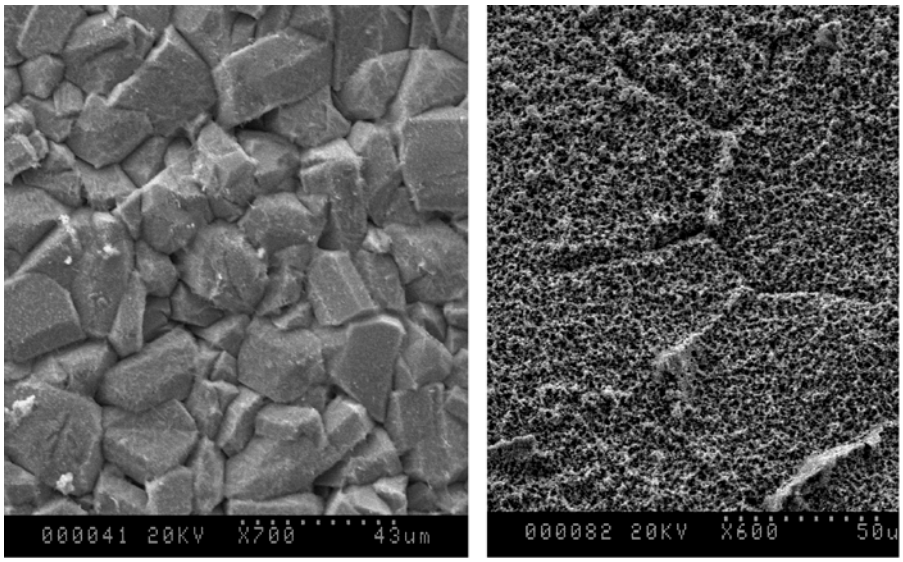


***Figure 1-12.*** *Surface morphology of copper specimen B before and after its corrosion film was removed in an ultrasonic bath; (a) – before; (b) – after. Test solution: 0.01 M $H_2S$ in water with deaeration. (Bhaskaran et al. 2013.)*

## 1.4 The work of Becker and Öijerholm 2017

Becker and Öijerholm studied copper in sulfide rich chloride containing deoxygenated water at 90 °C by slow strain rate testing (Becker and Öijerholm 2017).

### 1.4.1 Experimental

The copper material used in the testing was supplied to Studsvik by The Swedish Radiation Safety Authority (SSM). The copper material was part of a canister lid (TX214 HT1) which was supplied to SSM from the Swedish Nuclear Fuel and Waste Management Co (SKB). The material was oxygen-free phosphorus-containing copper (Cu-OFP). Before delivery to Studsvik, it had underwent the heat treatment cycle HT1. (SKB name of procedure, which is representative of all SKB's lids and bottoms. SKB developed a special heat treatment cycle for forged copper lids, known as HT1. At the beginning of the heat treatment, the copper lid is annealed in a nitrogen atmosphere at 450 °C for a holding time of 3 hours. The lid is then cooled in a nitrogen atmosphere in a furnace at 100 °C, followed by final cooling in air with the furnace door open (Jonsson and Ronneteg 2014).)

Figure 1-13 shows a drawing of test specimen used.

The tests were performed at about 4 atmospheres overpressure. The solution was 0.1 M NaCl with additions of a phosphate buffer to counter the alkalisation caused by sulfide additions and maintain a neutral pH (the exact composition of the buffer solution is not provided). Table 1-4 shows the sulfide concentrations applied and the resulting corrosion potentials for copper.

**Table 1-4. Average experimental data, and standard deviation, that were measured during the experiments (Becker and Öijerholm 2017).**

| Parameter | Exp1 | Exp2 | Exp3 | Exp4 | Exp5 |
|---|---|---|---|---|---|
| Sulfide (mM) | 0.8 | 0.8 | 0.07 | 0.06 | 0.003 |
| Corrosion potential (mV. vs SHE) | −736 | −637 | −580 | −575 | −387 |

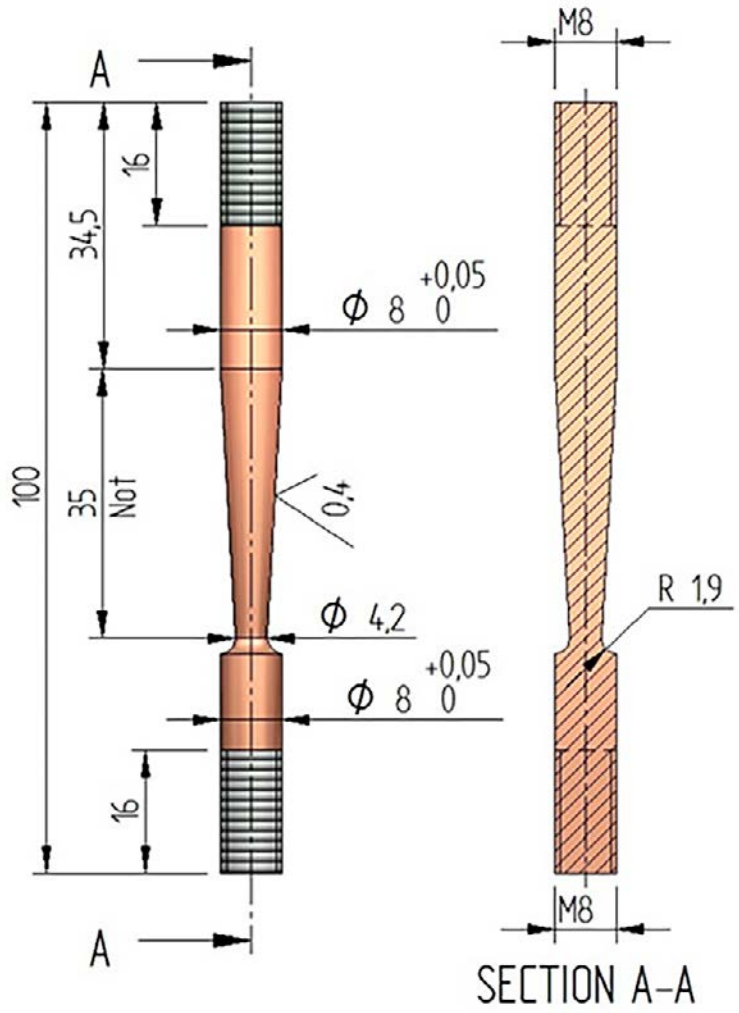


***Figure 1-13.*** *Drawing of the test pieces studied by Becker and Öijerholm 2017.*

A constant displacement rate was applied giving a strain rate of about $0.67 \times 10^{-7}$ $s^{-1}$ at the narrowest part of the test rods. The test rods were not drawn to fracture but were allowed to relax after a period of about 380 hours or about 15 days of straining.

### 1.4.2 Results

The results interpreted as signs of SCC all come from examination of the tested material using SEM. Figure 1-14 shows some surface features after test in Exp1 (upper two images) and Exp2 (lower two images), both experiments in 0.8 mM sulfide.

Figure 1-15 shows features found in cross section after test in Exp1. The number below the images show the distance between the feature and the narrowest part of the test specimen. (Becker and Öijerholm 2017.)

Figure 1-16 shows surface features after test in Exp4 in 0.06 mM sulfide. The appearance of the surface in Figure 1-16 can to be compared to the appearance in Figure 1-14 for 0.8 mM sulfide.

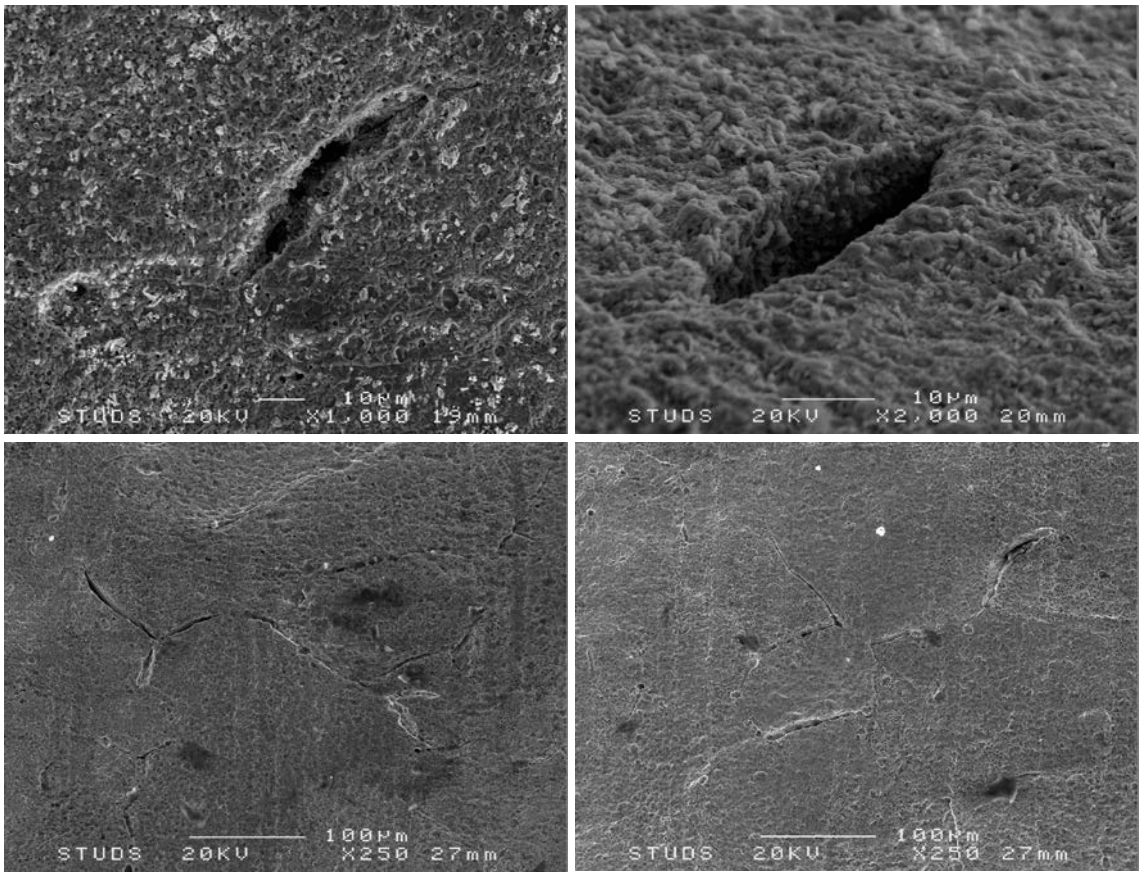


***Figure 1-14.*** *Surface features found after test in Exp1 (upper two images) and Exp2 (lower two images), both experiments in 0.8 mM sulfide. (Becker and Öijerholm 2017.)*

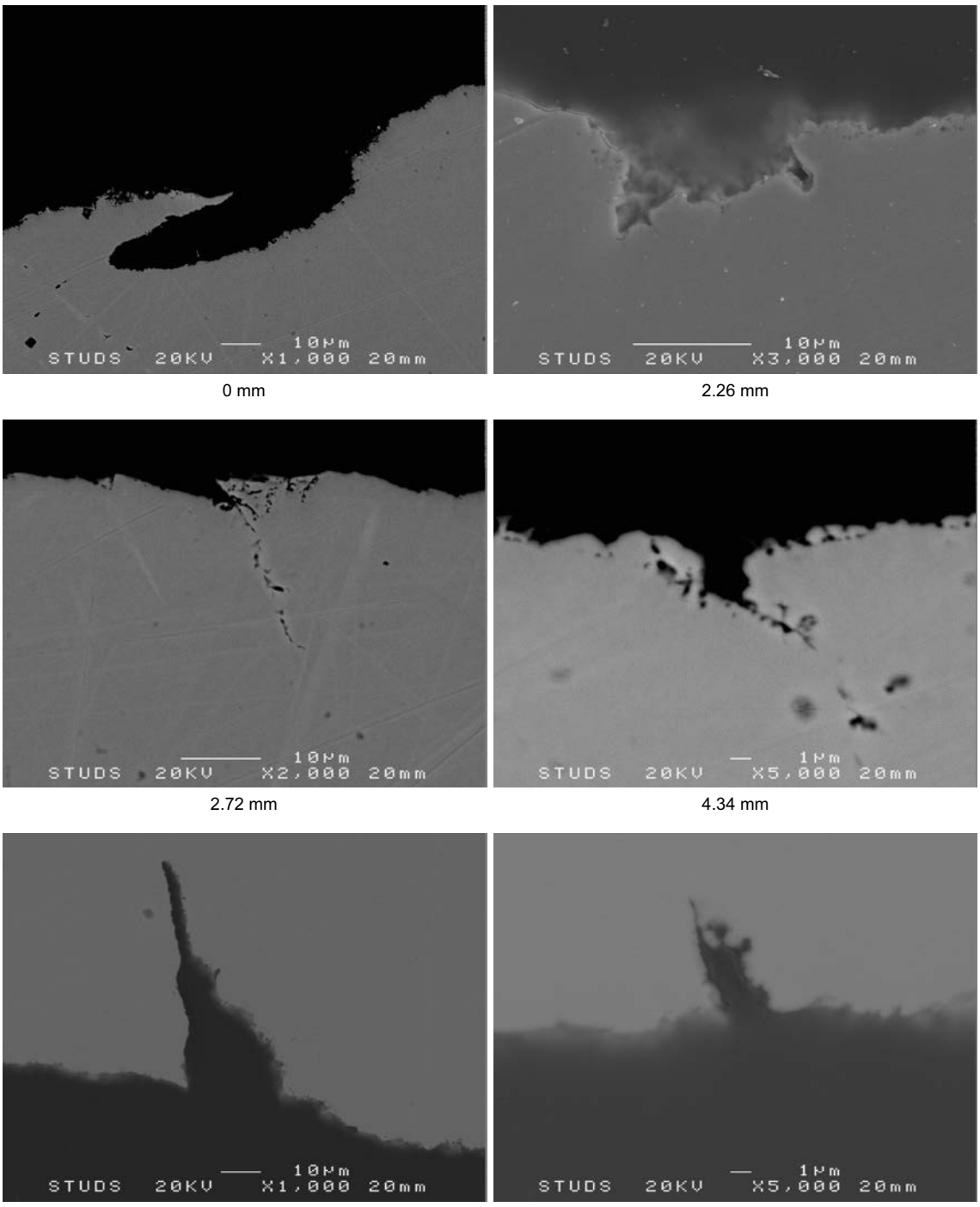


***Figure 1-15.*** *Features found in cross section after test in Exp1. The number below the images show the distance between the feature and the narrowest part of the test specimen. (Becker and Öijerholm 2017.)*

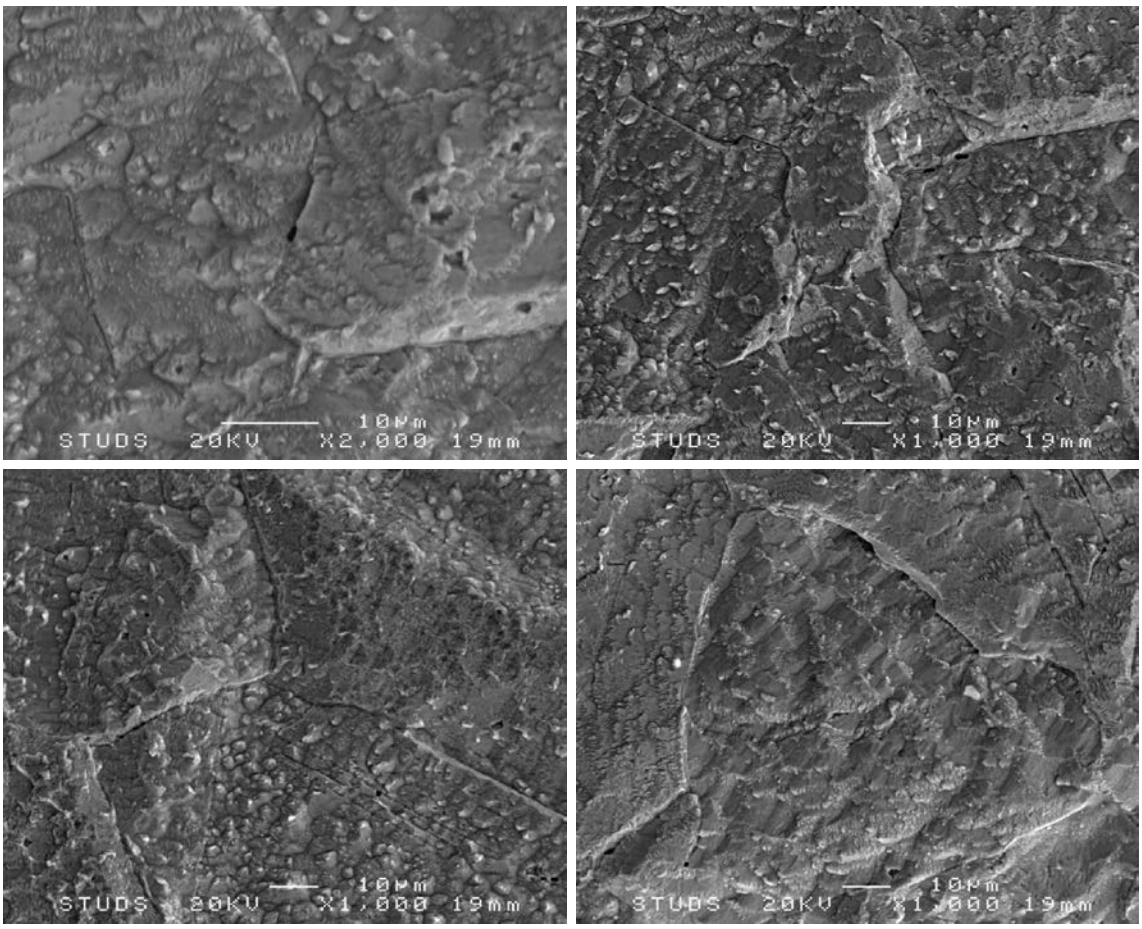


***Figure 1-16.*** *Surface features after test in Exp4 in 0.08 mM sulfide. (Becker and Öijerholm 2017.)*

## 1.5 Stress corrosion cracking of copper in nitrous/nitric media

The appearance of SCC in copper is not necessarily the same in one environment as in another, but it may be useful to look at signs of SCC from studies where nitrous or nitric compounds are likely to have been the promoting agent for SCC.

Clear evidence of stress corrosion cracking of copper has been found in concentrated nitrate solutions. Farina et al. (2005) studied stress corrosion cracking of pure copper at room temperature in 1 M $Cu(NO_3)_2$ aqueous solution. They report an appearance of the surface with a multitude of small parallel cracks. The cracks are clearly visible in SEM micrographs (Farina et al. 2005).

Kužnicka and Junik (2007) made a case study of a failed copper tube. The failed tube was made of Cu-DHP (C12200) in hard temper, according to ASTM B 280. Chemical composition was determined by chemical analysis (% w/w): (Cu + Ag) 99.95, P 0.040, Fe 0.0005, Ni 0.0005, Pb 0.0005, Sb 0.001, Zn 0.003, Bi 0.0005, As 0.0005, S 0.0011.

The inside medium was freon but the pipe was evidently cracked from the outside which was a sand-concrete mixture. Water extracts from the sand was found to contain about 2.6 mg/l of ammonia which was believed to have caused the cracking together with residual stress. The cracking seems to be intergranular, mainly, with branching cracks.

In conclusion, cracks in copper can occur both as singular branching cracks, possibly initiated from a corrosion pit (Kužnicka and Junik 2007) and as a multitude of cracks in the surface under strain (Farina et al. 2005), other prerequisites for cracking being present. It should be emphasised that in both cases nitric or ammonium agents were concluded to have been necessary for the cracking.

# 2 Experimental

## 2.1 Equipment and test procedure

Modified artificial sea water was made using the ASTM D1141 artificial sea water (ASW) standard as the base recipe, and was used for the tests at room temperature. In the modified artificial sea water all chlorides was exchanged to NaCl due to possible unwanted precipitation of $CaCO_3$(s), in the solution when alkaline $Na_2S$ stock solution was added to the original standard artificial sea water. The chloride concentration of the modified artificial sea water (MASW) was kept equal to the concentration in the ASTM D1141 standard. This modified artificial sea water was used for the tests in 80 °C.

The SSRT machine used at Swerea KIMAB AB for the copper test is made by Cortest Incorporated and is capable in the current set up to withstand loads up to 2 000 kg. The strain rate used was $10^{-6}$ $s^{-1}$ which is normally used at Swerea KIMAB AB and is just slightly faster than in the work of Taniguchi and Kawasaki. Bhaskaran et al. used the strain rate $10^{-6}$ $s^{-1}$ in some of their experiments. The SSRT-setup is shown in Figure 2-1.

Pre-moistured nitrogen (the nitrogen was bubbled through deionised water) was continuously bubbled through the modified artificial sea water in the SSRT-cell during all the tests, to keep the oxygen level at a minimum. By doing so there was though a risk that the $Na_2S$–concentration would be reduced gradually due to $H_2S$ leaving the solution via the nitrogen outlet. The $Na_2S$–concentration would also be additionally reduced, using this setup, by reaction with the copper sample during the test. The target sulfide concentration was 0.01 M (= 10 mM or 320 mg/l).

To ensure that the concentration of $Na_2S$ stays at 0.01 M during the experiments a special setup with continuous flow of solution was used. Figure 2-2 shows a schematic sketch of this setup. The setup consists of a 10 litres reservoir filled with test solution. The outlet valve is adjusted so that gravitation feeds a slow flow through the SSRT-cell ending up in a reservoir for used test solution. A small overpressure of nitrogen gas is maintained.

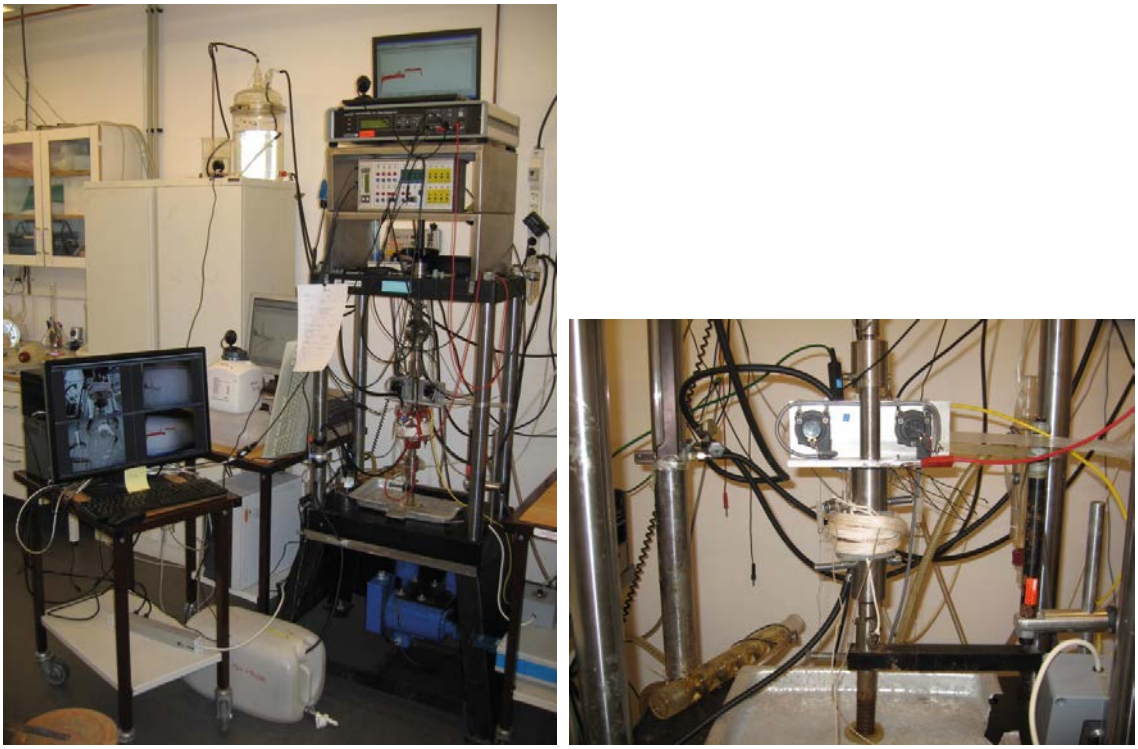

***Figure 2-1.*** *The SSRT-machine and all the surrounding equipment, to the left, from the study of the round test rods. To the right is a photo of the SSRT-part of the equipment as it was used in the tests of the test rods with rectangular cross section.*

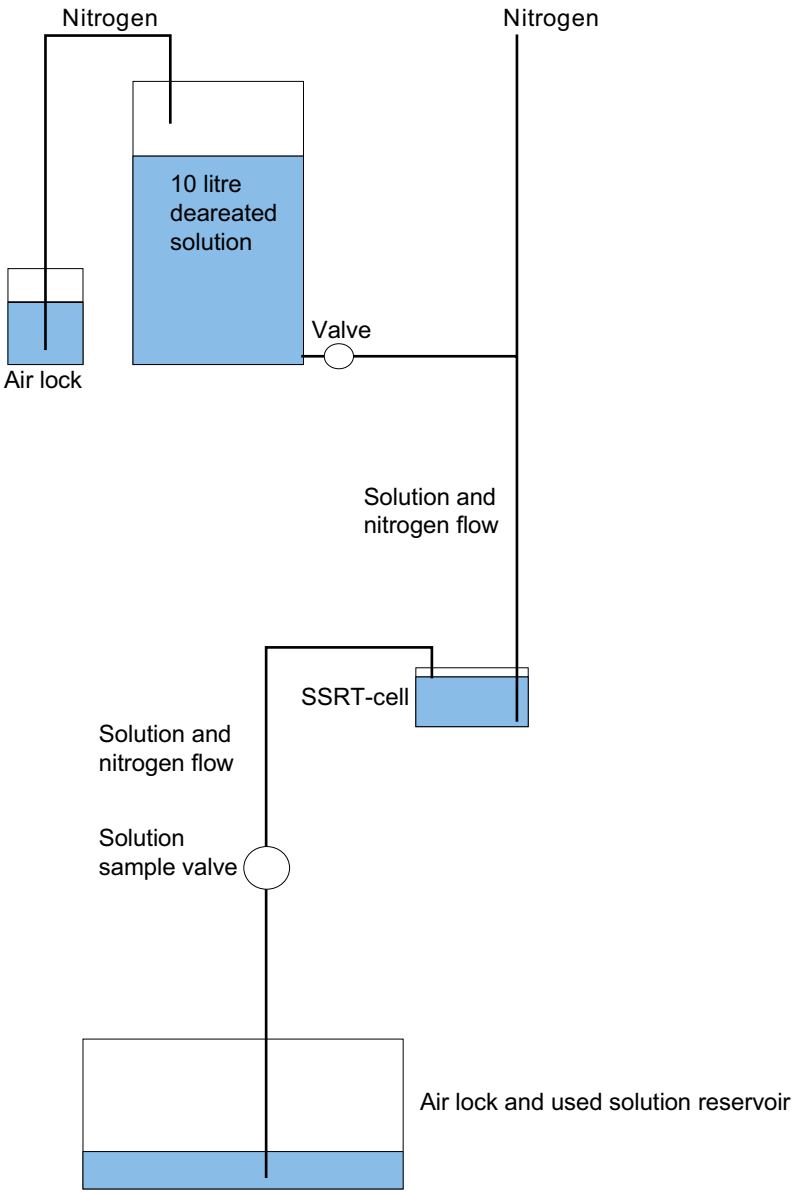


***Figure 2-2.*** *Schematic sketch of the solution flow system during SSRT-test on copper.*

**Procedure:**

The whole setup including reservoir containing modified artificial sea water, SSRT-cell (no solution in the cell at this moment) and all tubes was flushed with pre-moist nitrogen 24 hours before start of each experiment. One hour before the SSRT-test containing $Na_2S$ started, a measured amount (0.78 g/litre) of $Na_2S$ was swiftly added via a funnel into the reservoir filled with modified artificial sea water. During this hour the $Na_2S$ was dissolved by means of the nitrogen bubbling in the reservoir. At the start of the SSRT-test the solution was poured down to the SSRT-cell via a hose and when the cell was filled up the flow was adjusted to approximately 1 litre/24 hours. (This flow was later increased to approximately 4 litres/24hours, the last 24 hours due to a slightly lower level of sulfide when measured than wished.) The nitrogen flow was then reduced to a minimum in the whole setup combining and preserving low oxygen level and low $H_2S$-loss.

A solution sample valve was situated between the SSRT-cell and the used solution reservoir. The solution samples taken there, were immediately analyzed of its sulfide content by means of CHEMetrics sulfide analyzing vacuum glass kit. Figure 2-3 shows the tubes from the sulfide analyzing kit.

Before the SSRT-testing began the oxygen level in the cell was measured under realistic forms using a Hamilton optical oxygen measuring device. (An optical system does not consume oxygen during measurement.) There was no place on the SSRT-cell for an oxygen sensor during the actual SSRT-tests. The oxygen level test on the SSRT setup showed that the setup could achieve low oxygen levels during the SSRT-test. On an isolated SSRT-cell the oxygen level leveled out at 7 ppb. On the whole setup the level leveled out at 30 ppb. Results of oxygen measurements are shown in Figure 2-4.

The corrosion potential (ref: Ag/AgCl, double junction) was measured during the SSRT tests. During all experiments there was also a Pt-wire in contact with the test solution. All potentials are reported on the SCE scale. After the SSRT measurements all tested specimens were studied by light optical microscopy and by scanning electron microscopy

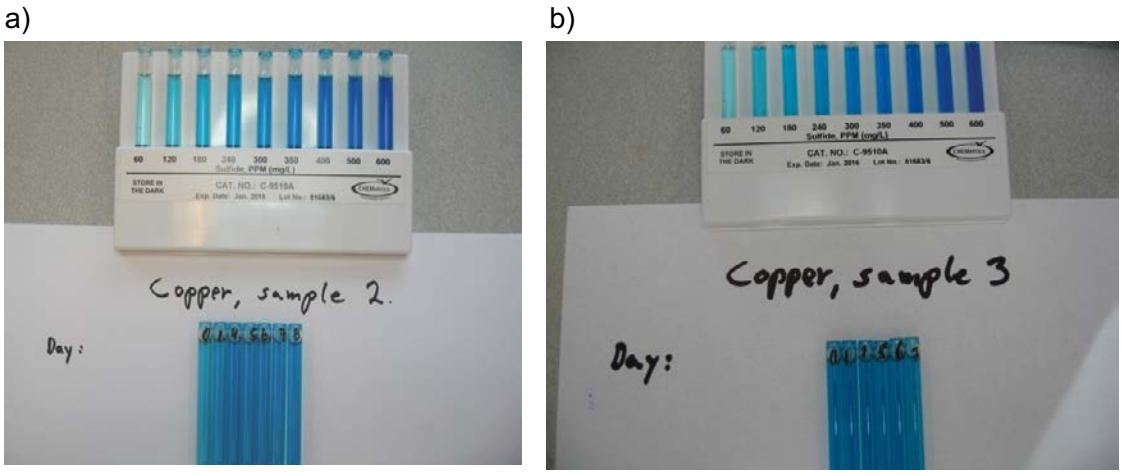


***Figure 2-3.*** *The tubes from the sulfide analyzing vacuum glass kit test. Samples collected during a test in a) artificial sea water at room temperature, b) modified artificial sea water at 80 °C (b). The target concentration was 0.01 M sulfide (320 mg/l), in both cases.*

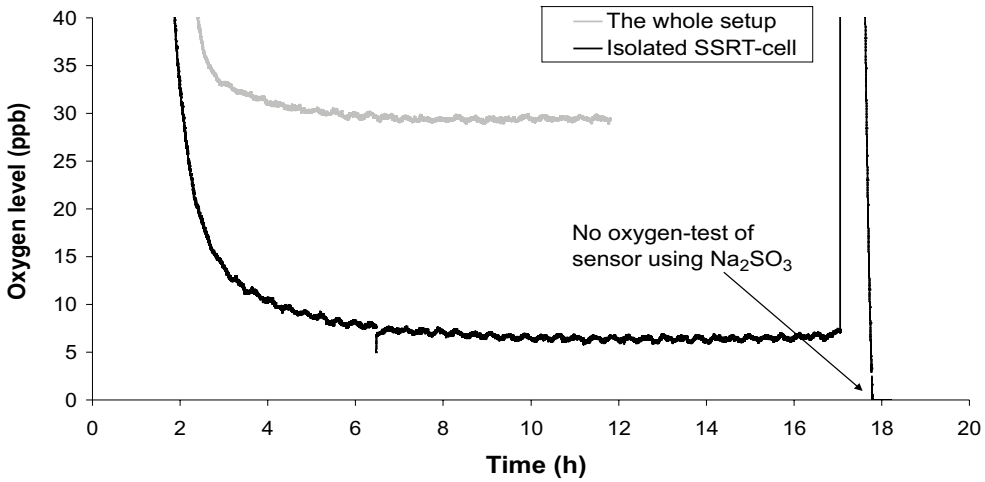


***Figure 2-4.*** *In an isolated SSRT-cell the oxygen level leveled out at 7 ppb. On the whole setup the level leveled out at 30 ppb. In the end of the "Isolated SSRT-cell"-test the sensor was placed in an environment where $Na_2SO_3$ was used as an oxygen scavenger.*

## 2.2 Hardness of rolled copper after heat treatment

The copper material from rolling and machining to rectangular test rods was found to be very hard. A series of heat treatment was performed to decrease the hardness of the material to give a strain at rupture similar to that of Taniguchi and Kawasaki (2008). A target hardness was estimated to 60 HV1 and the Vickers hardness was measured of test pieces after selected heat treatments. Figure 2-5 shows the Vickers hardness after each heat treatment.

The round test rods were fully annealed before testing (Specimens 1-5). 10 minutes at 600 °C was considered to give fully annealed conditions. The flat test rods in tests 6 and 7 had the hardness of the cold rolled material and the flat test rods in test 8 and 9 had the hardness resulting from 10 minutes at 381 °C followed by water quenching. (The water quenching lasted for about 30 s, or until the specimen could be touched by hand.)

## 2.3 Composition of the copper materials tested

Table 2-1 shows the composition of the copper materials used in the present study and in the referenced studies. No exact composition is available for the material studied by Bhaskaran et al. However, the material is known to originate from SKB and the composition is likely to be similar to that studied by Becker and Öijerholm and to that used in the present study. The material studied by Taniguchi and Kawasaki comes from a different source.

**Table 2-1. Composition of the copper materials used in the present study and in the referenced studies.**

| Chemical content (wt-ppm) | Taniguchi and Kawasaki | Becker and Öijerholm | This work |
|---|---|---|---|
| P | 45 | 43–60 | 57–70 |
| Pb | 1.9 | < 1 | < 1 |
| Bi | < 1 | < 1 | < 1 |
| As | | < 1 | < 1 |
| Sb | | < 1 | < 1 |
| Sn | | < 0.5 | < 0.5 |
| Zn | < 1 | < 1 | < 1 |
| Mn | | < 0.5 | < 0.5 |
| Cr | | <1 | < 1 |
| Co | | <1 | < 1 |
| Cd | < 1 | <1 | < 1 |
| Fe | | <1 | < 1 |
| Ni | | 2 | 2 |
| Ag | | 12 | 12 |
| Se | < 1 | < 1 | < 1 |
| Te | < 1 | < 1 | < 1 |
| S | < 1 | 6 | 6 |
| Hg | < 1 | | |
| O | 3 | | |
| H | 0.4 | | |

The main differences in the composition from SKB-copper seem to be that the material studied by Taniguchi and Kawasaki contained very little sulfur and no analysis for silver is reported.

The round test rods were cut from the canister material and turned into the desired form. Figure 2-6 shows the drawing.

Figure 2-7 shows a photo of a new round test rod and a test rod drawn to fracture in artificial seawater, for a reference curve.

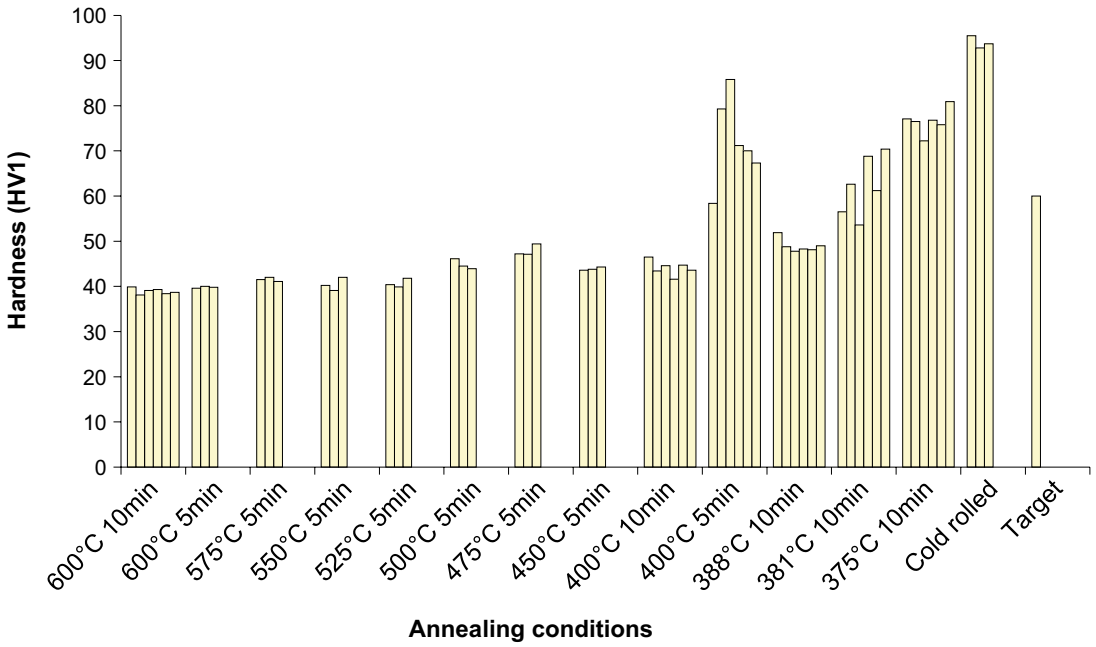


***Figure 2-5.*** *Vickers hardness of the copper material from cold rolling after various heat treatments. The target hardness was estimated from the apparent hardness of the material studied by Taniguchi and Kawasaki (2008).*

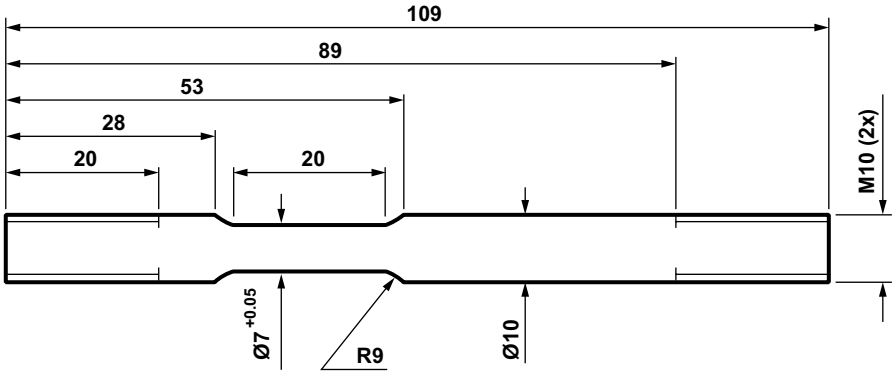


***Figure 2-6.*** *Drawing for the round test rods.*

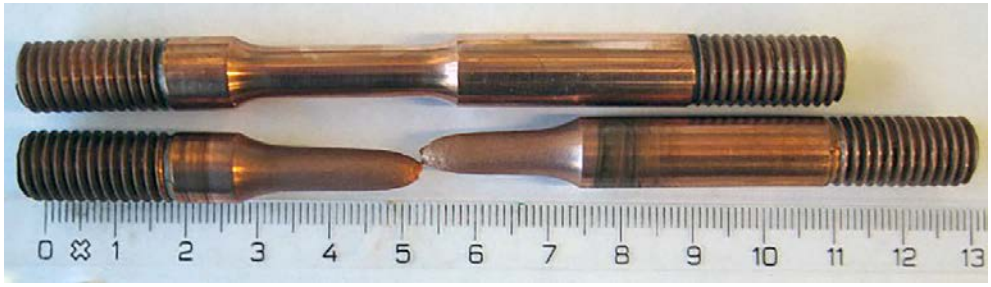


***Figure 2-7.*** *A photo of a new test rod and a test rod drawn to fracture in artificial seawater, for a reference curve.*

Rectangular test rods were cut to the dimensions in Figure 1-1. Figure 2-8 shows a photo of a rectangular test rod before testing. The material was cold rolled to the desired thickness, heat treated to reduce the hardness (not for all tests) and cut to form by milling. The final polish was made using diamond paste 3 µm just as in the work of Taniguchi and Kawasaki.

## 2.4 Test matrix

Table 2-2 shows a summary of the SSRT-tests performed in this study.

**Table 2-2. Test ID No, specimen shape, heat treatment before testing and test conditions.**

| Test specimen No and cross section shape | Heat treatment | Target sulfide concentration (mM) | Test temperature (°C) |
|---|---|---|---|
| 1 Round | 600 °C, 10 minutes | 0 | RT |
| 2 Round | 600 °C, 10 minutes | 10 | RT |
| 3 Round | 600 °C, 10 minutes | 10 | 80 |
| 4 Round | 600 °C, 10 minutes | 0 | 80 |
| 5 Round | 600 °C, 10 minutes | 0 | 80 |
| 6 Rectangular | No | 0 | 80 |
| 7 Rectangular | No | 10 | 80 |
| 8 Rectangular | 381 °C, 10 minutes | 0 | 80 |
| 9 Rectangular | 381 °C, 10 minutes | 10 | 80 |

***Figure 2-8.*** *A photo of a rectangular test rod rectangular test rod before testing.*

# 3 Results

## 3.1 Round Test Rods at Room Temperature

### 3.1.1 Stress-strain curves

Figure 3-1 shows the stress-strain curves for round copper rods in artificial sea water (ASW) at room temperature. The red curve shows the result for an addition of 10 mM sulfide and the black curve shows the result without sulfide addition.

No significant difference between the curve with sulfide addition and the curve without sulfide addition can be seen in Figure 3-1.

### 3.1.2 Corrosion potential

Figure 3-2 shows the corrosion potential for the copper test rod and the potential for a platinum wire in the same solution, a) without $Na_2S$, b) with 0.01 M $Na_2S$.

Figure 3-2 shows that the potential of Pt in experiment 1 is close to 0 mV mV vs. SCE in artificial sea water without sulfide. The potential of the copper test rod is approximately −300 mV vs. SCE. The addition of 10 mM sulfide to artificial sea water, experiment 2, shifts the potentials to between −1 000 and −900 mV for the copper test rod and to about −600 mV for Pt.

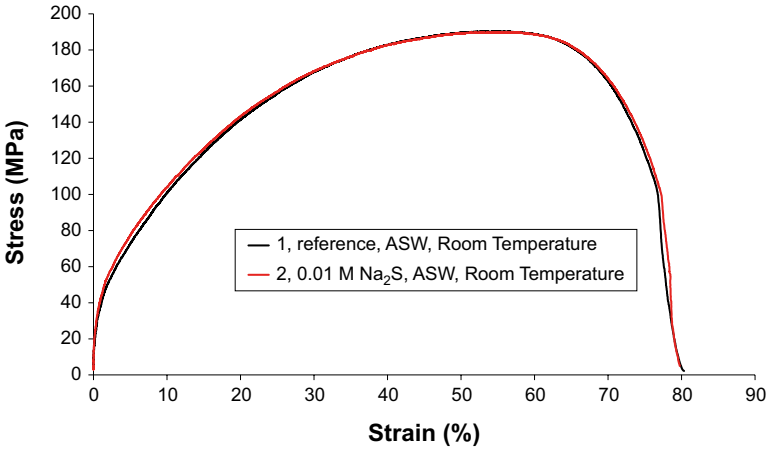


***Figure 3-1.*** *Stress-strain curves for copper in artificial sea water (ASW) at room temperature, with and without 0.01 M $Na_2S$.*

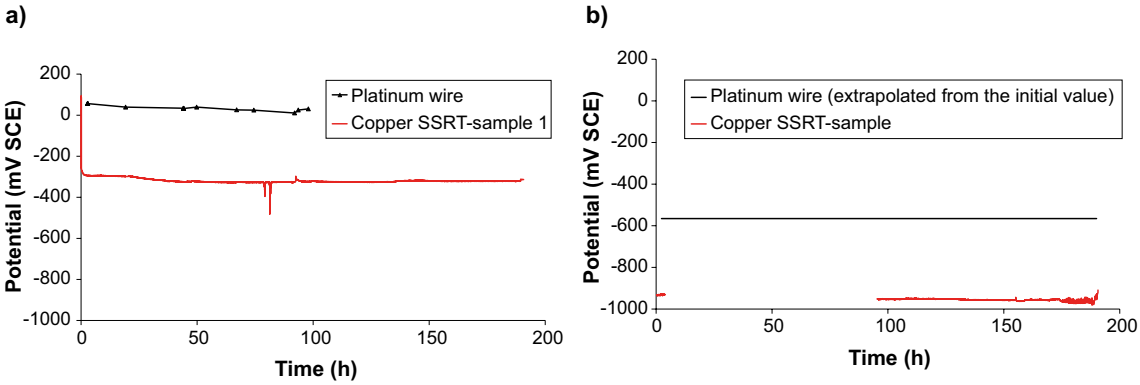


***Figure 3-2.*** *Corrosion potentials and Pt potentials measured during SSRT-test at room temperature, a) without $Na_2S$, b) with 0.01 M $Na_2S$.*

### 3.1.3 Sulfide concentrations

Figure 3-3 shows the sulfide concentrations in the sampled outlet solution. As mentioned in Section 2-1, the method for measuring sulfide concentration is rather coarse but Figure 3-3 shows that the concentration remains constant during the test.

Figure 3-3 is representative of all the sulfide measurements for tests in 10 mM sulfide solutions.

## 3.2 Round Test Rods at 80 °C

### 3.2.1 Stress-strain curves

Figure 3-4 shows the stress-strain curves for round copper rods in modified artificial seawater (MASW) at 80 °C. The red curve shows the result for an addition of 10 mM sulfide and the black curve and the blue curve show the result without sulfide addition. The difference between the black curve and the blue curve indicates the level of reproducibility of the stress-strain curves. The curves for room temperature from Figure 3-1 are included as dashed lines, for comparison.

### 3.2.2 Corrosion potentials

Figure 3-5 shows the corrosion potential for the copper test rod and the potential for a platinum wire in the same solution, a) without $Na_2S$, b) with 0.01 M $Na_2S$.

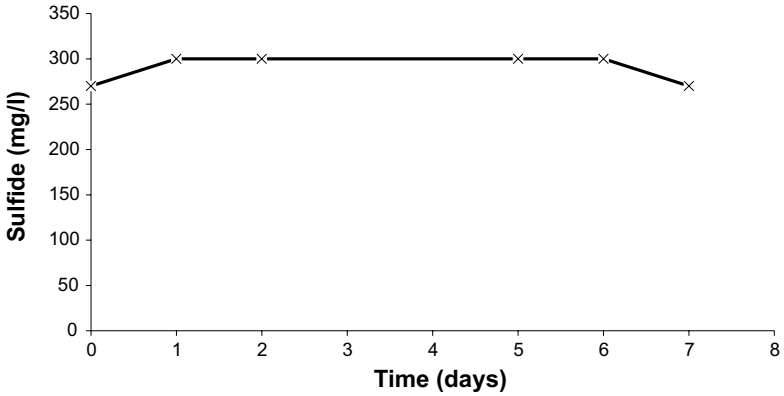


***Figure 3-3.*** *Sulfide concentrations in the sampled outlet solution.*

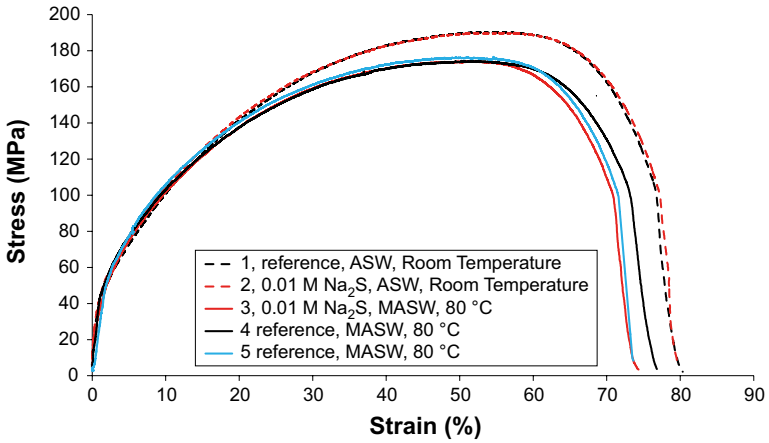


***Figure 3-4.*** *Stress-strain curves for copper in modified artificial sea water (MASW) at 80 °C, with (red curve) and without (black curve and blue curve) 10 mM $Na_2S$. The corresponding curves for room temperature are included as dashed lines, for comparison.*

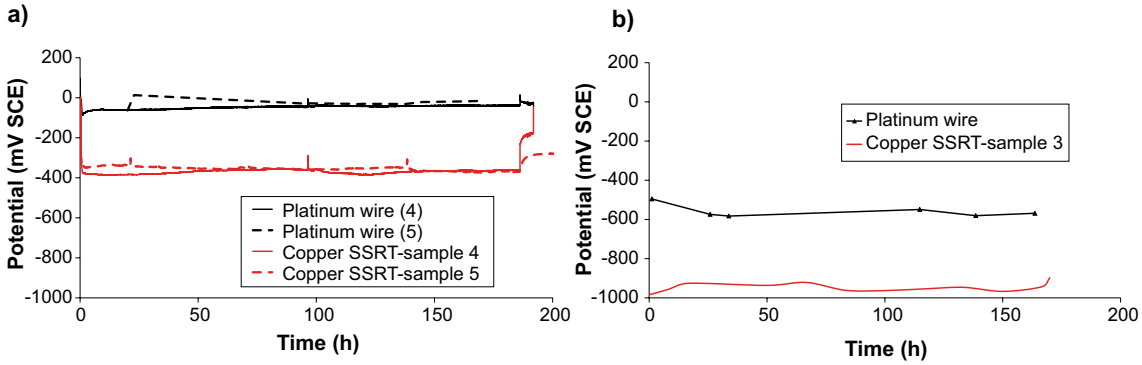


***Figure 3-5.*** *Corrosion potentials and Pt potentials measured during SSRT-test at 80 °C, a) without $Na_2S$, b) with 10 mM $Na_2S$.*

Figure 3-5 shows that the potential of Pt in experiment 4 and 5 are relatively constant between 0 and −100 mV vs. SCE in artificial sea water without sulfide. The potentials of the copper test rods are approximately −400 mV vs. SCE. The addition of 10 mM sulfide to artificial sea water shifts the potentials to between −1 000 and −900 mV for the copper test rod and to about −600 mV for Pt.

## 3.3 Rectangular Test Rods at 80 °C before heat treatment

### 3.3.1 Stress-strain curves

Figure 3-6 shows stress-strain curves for rectangular test rods in modified artificial sea water (MASW) at 80 °C, with (red curve) and without (black curve) 10 mM $Na_2S$.

Figure 3-6 shows no significant effect of the addition of 10 mM sulfide on the stress-strain curves.

### 3.3.2 Corrosion Potentials

Figure 3-7 shows the corrosion potential for the copper test rod and the potential for a platinum wire in the same solution, a) without $Na_2S$, b) with 0.01 M $Na_2S$.

Figure 3-7 shows potentials that are slightly higher than in experiments 5 and 6 in modified artificial seawater without sulfide addition (Figure 3-5a). The potentials in artificial seawater with 10 mM sulfide are relatively constant at about −600 mV and −1 000 mV for Pt and the copper test rods, respectively. These values are similar to those in Figure 3-5b for round test rods.

## 3.4 Rectangular Test Rods at 80 °C after heat treatment

### 3.4.1 Stress-strain curves

Figure 3-8 shows the stress-strain curves for the test rods with rectangular cross section after heat treatment. The curves for the material obtained before heat treatment are included as dashed lines, for comparison.

### 3.4.2 Corrosion Potentials

Figure 3-9 shows the corrosion potential for the copper test rod and the potential for a platinum wire in the same solution, a) without $Na_2S$, b) with 0.01 M $Na_2S$.

The higher noise level in Figure 3-9a compared to Figures 3-5a and 3-7a is probably related to the difficulty in sealing the experimental cell around the rectangular cross section of the test rods. This sealing may have been less successful in this particular test.

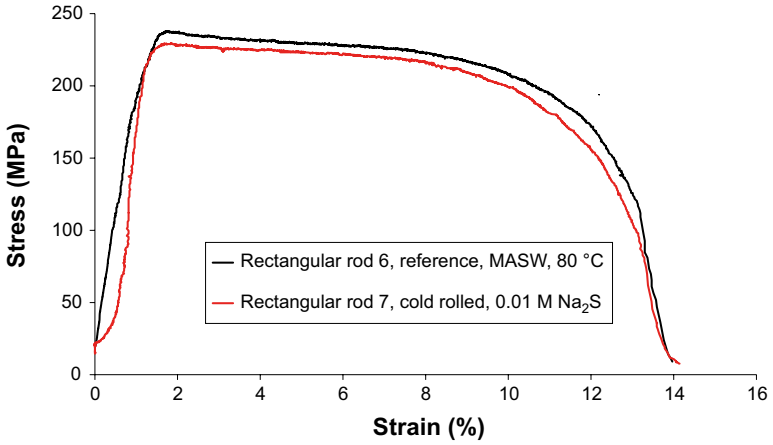


***Figure 3-6.*** *Stress-strain curves for copper in modified artificial sea water (MASW) at 80 °C, with (red curve) and without (black curve) 10 mM $Na_2S$.*

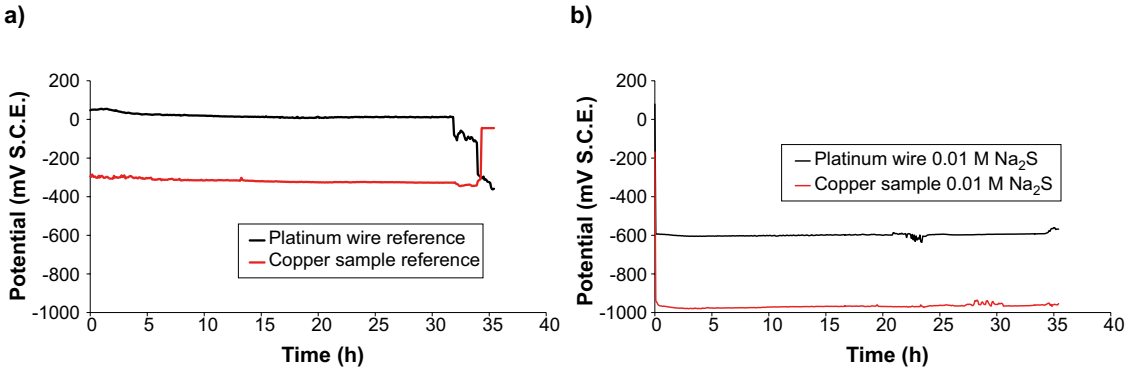


***Figure 3-7.*** *Corrosion potentials and Pt potentials measured during SSRT-test at 80 °C, a) without $Na_2S$, b) with 10 mM $Na_2S$*

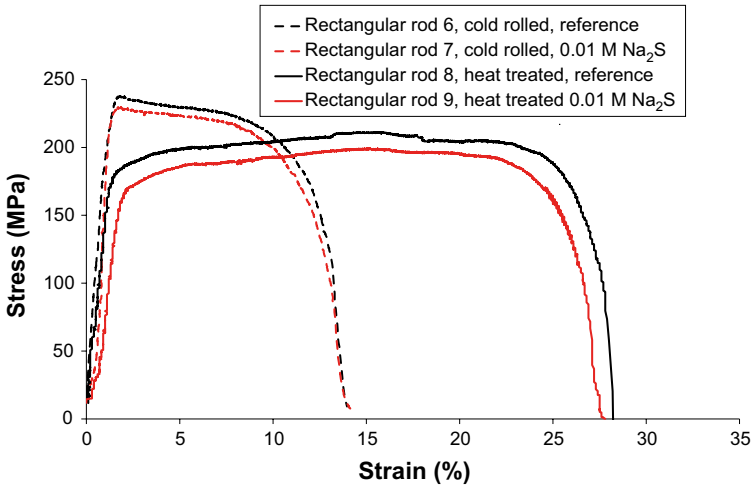


***Figure 3-8.*** *Stress-strain curves for copper in modified artificial sea water (MASW) at 80 °C, with (red curve) and without (black curve) 10 mM $Na_2S$. The curves for the material obtained before heat treatment are included as dashed lines, for comparison.*

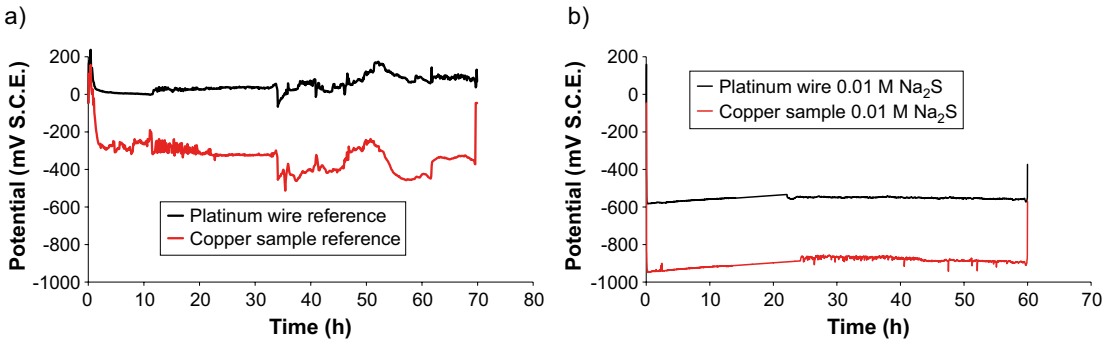


***Figure 3-9.*** *Corrosion potentials and Pt potentials measured during SSRT-test at 80 °C, a) without $Na_2S$, b) with 10 mM $Na_2S$.*

## 3.5 Metallographic examinations

Figure 3-10 shows an assembly of images for the round test rod tested in 10 mM sulfide at room temperature in test 2 (see Table 2-2). For comparison, Figure 3-11 show an assembly of images of the test rod from test 1, without sulfide. Figure 3-10 shows some kind of surface feature or defect as a dark oval close to the fracture zone. The dark oval is shown in gradually increasing magnification as indicated by the white arrows. Some dark streaks along the test rod can be seen in the lower right hand image. Similar dark streaks can be seen also in Figure 3-11.

Figure 3-12 shows an assembly of images for the round test rods tested in 10 mM sulfide at 80 °C in test 3. The upper image shows flaking corrosion products at the right hand side. Two special features at the fracture zone are shown with gradually increased magnification. Figure 3-13 shows an assembly of images from the same test piece as Figure 3-12. The images show the site where corrosion products are flaking off and reveal a pattern of what looks like superficial grain boundary corrosion.

Figure 3-14 shows images of the fracture surface of the same test piece as Figures 3-12 and 3-13. The images show the dimpled appearance usually associated with ductile fracture.

Figure 3-15 shows an assembly of images for the test rod with rectangular cross section tested in 10 mM sulfide at 80 °C in test 7. The material was not annealed after cold rolling and fractured at about 14 % strain (Figure 3-8).

The images in Figure 3-15 show cracked corrosion products and parts of the surface where the corrosion products apparently have flaked off. The copper metal visible where corrosion products seem to have flaked off does not show any cracks. Figure 3-16 shows an assembly of images of the test rod for test 9 in synthetic seawater with 10 mM sulfide at 80 °C. The material here was annealed after cold rolling and fractured at about 28 % strain (Figure 3-8). The appearance of cracked corrosion products is more pronounced in Figure 3-16 than in Figure 3-15. No cracks in the metal beneath the corrosion products are visible in Figure 3-16. Images of the same test rod after removal of the corrosion products with HCl are shown in Figure 3-17. The lower two images show a feature that may be an initial defect in the material, possibly from the rolling operation or from the casting of the material. The right hand edge of the specimen in the lower left image in Figure 3-17 shows an edge where it looks like copper metal has been smeared over a defect at the edge. Thus, the images indicate that the polishing of the edge of the test rod before testing was not perfect. The central feature in the lower right hand image has some similarities with features in the images in Figure 1-14 from Becker and Öijerholm (2017).

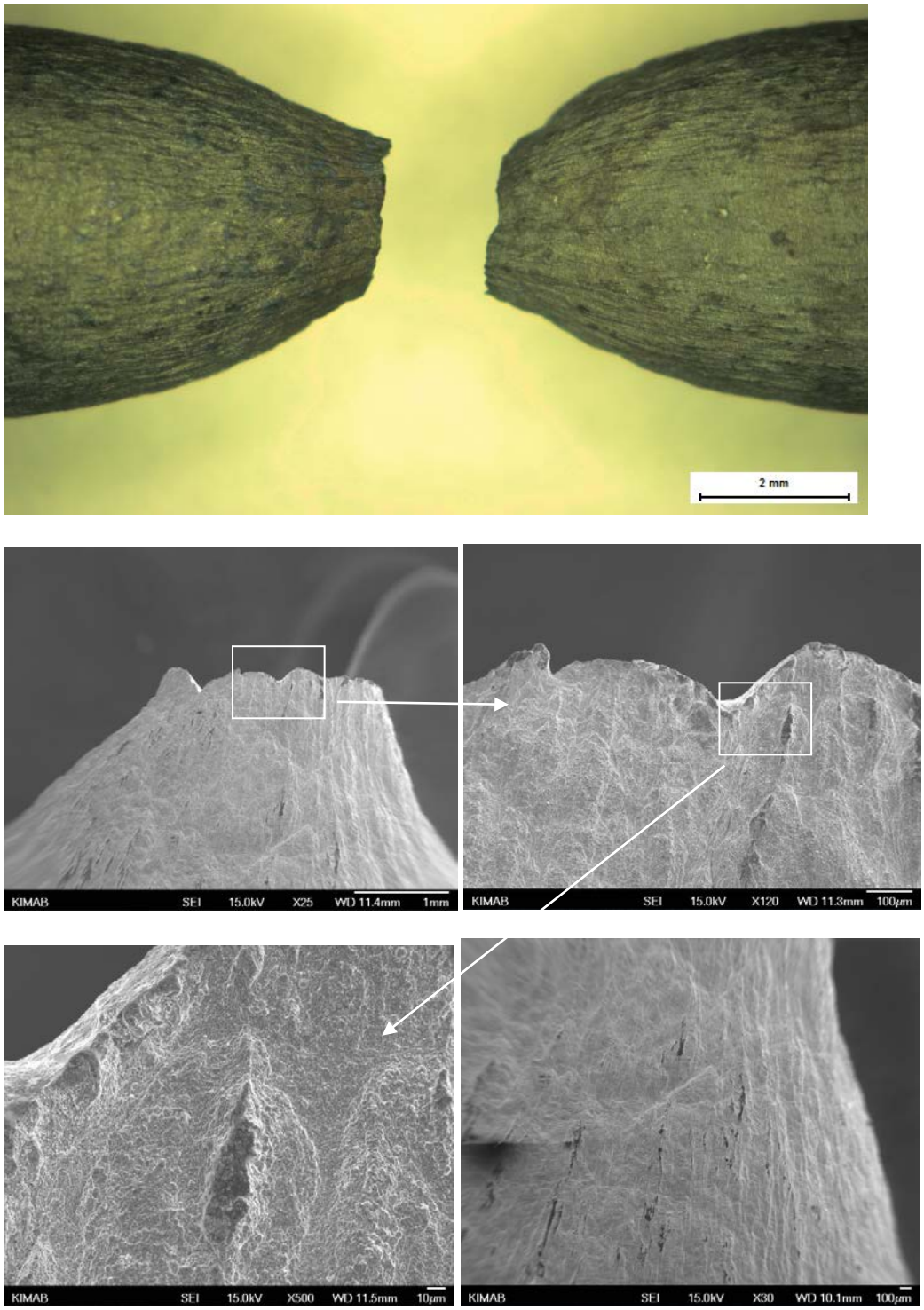


***Figure 3-10.*** *An assembly of images of the fracture zone for test 2 in synthetic seawater with 10 mM sulfide at room temperature.*

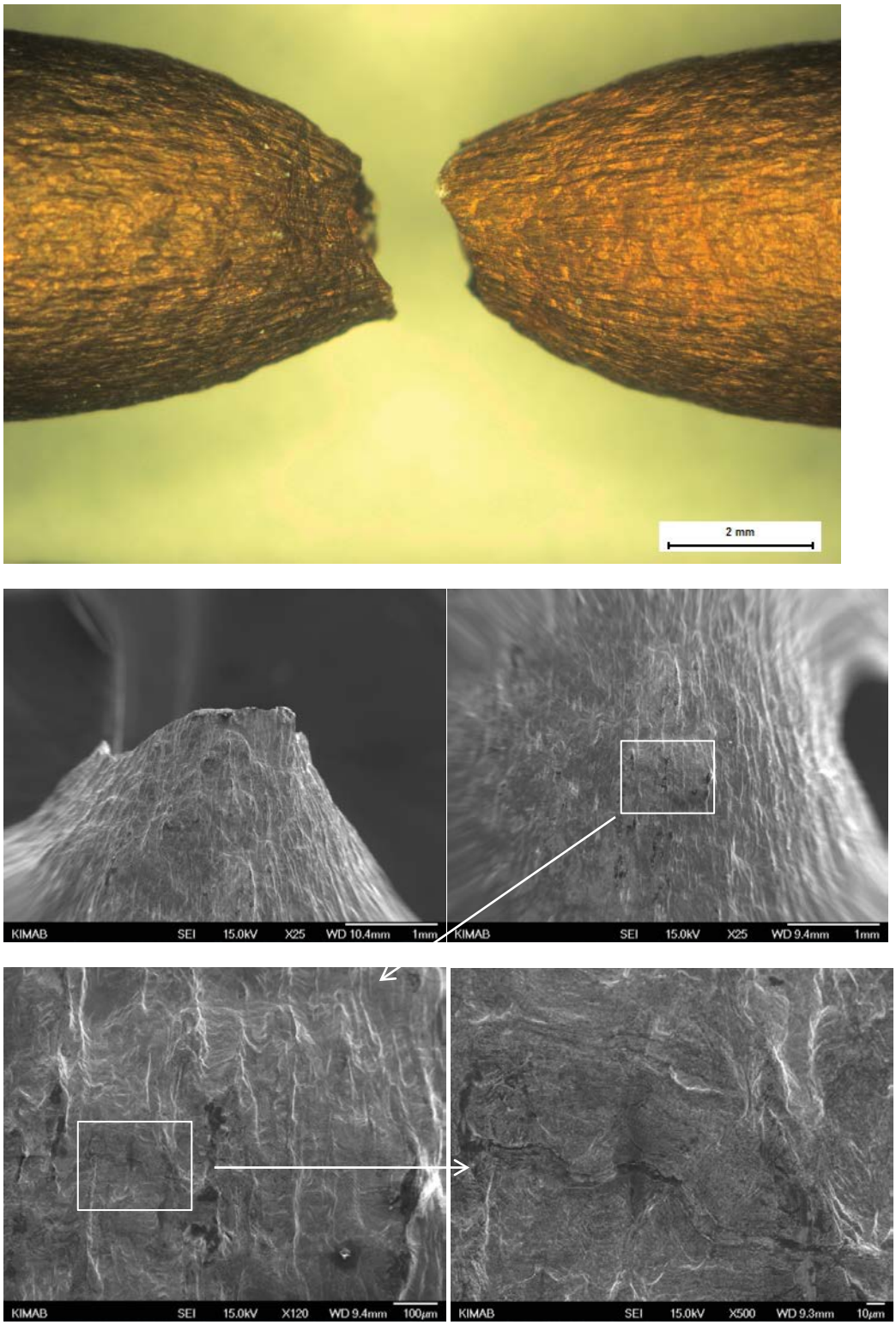


***Figure 3-11.*** *An assembly of images of the fracture zone for test 1 in synthetic seawater at room temperature.*

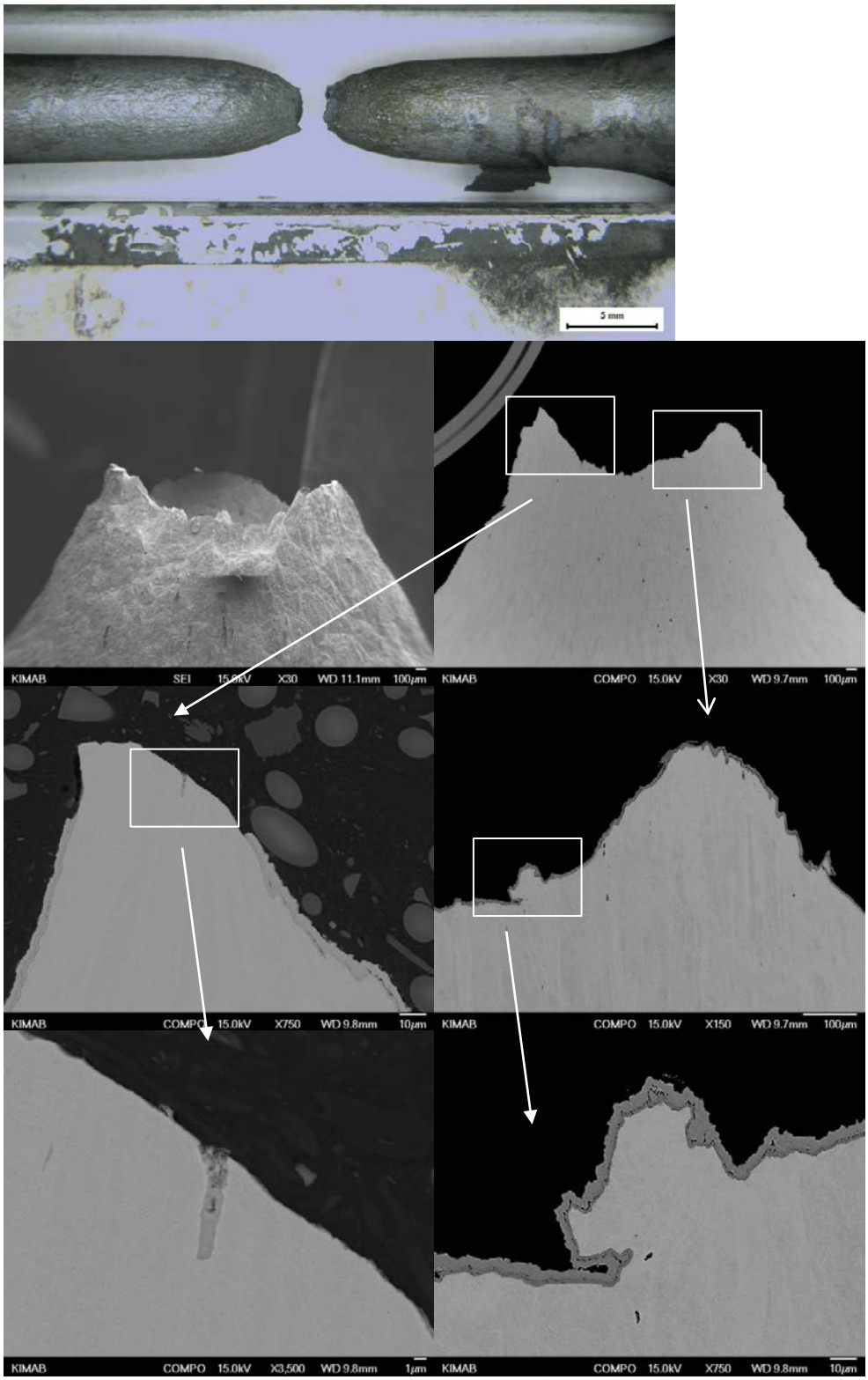


***Figure 3-12.*** *An assembly of images of the fracture zone for test 3 synthetic seawater with 10 mM sulfide at 80 °C.*

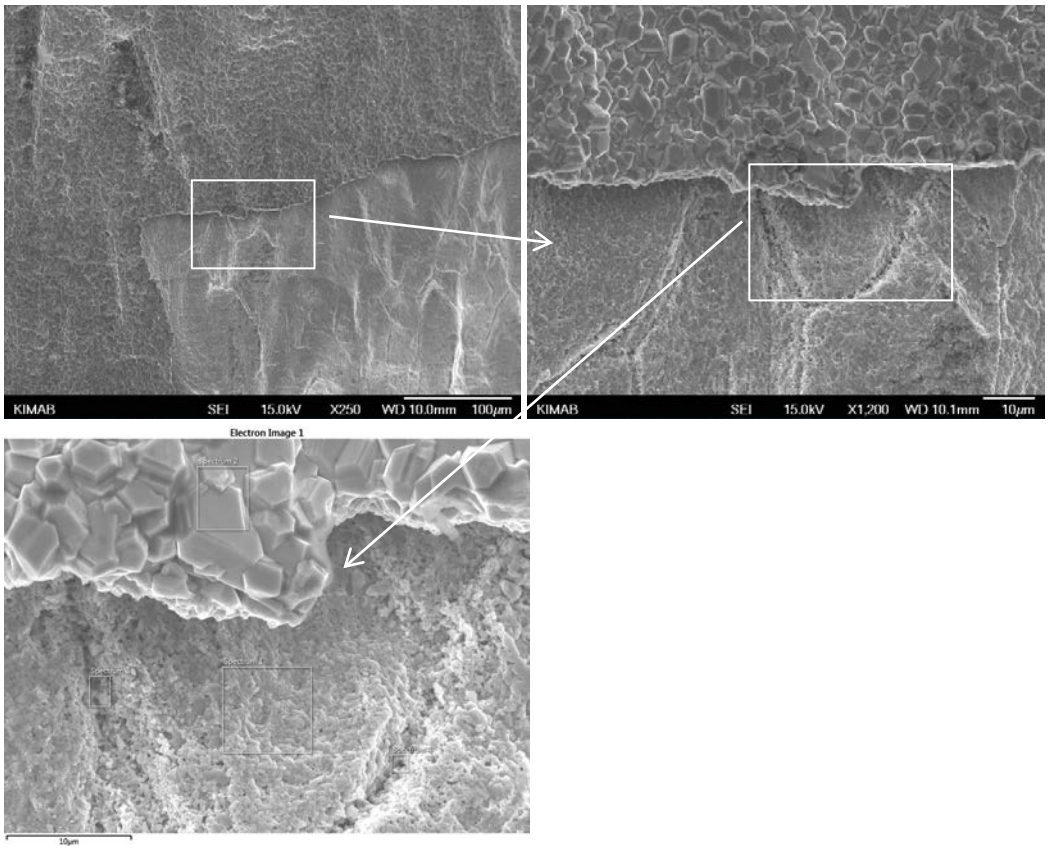


***Figure 3-13.*** *Surface features found after SSRT test in 10 mM sulfide at 80 °C.*

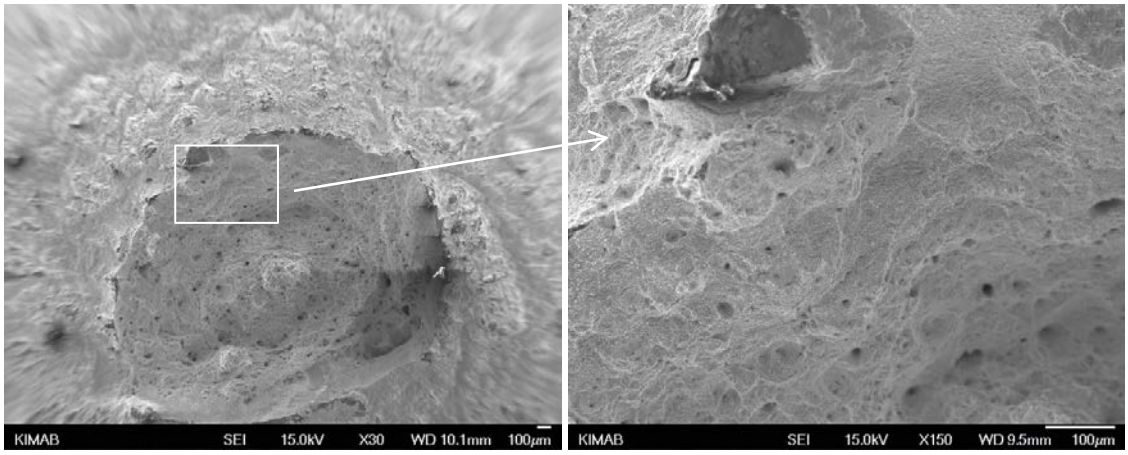


***Figure 3-14.*** *Appearance of the fracture surface after SSRT test in 10 mM sulfide at 80 °C.*

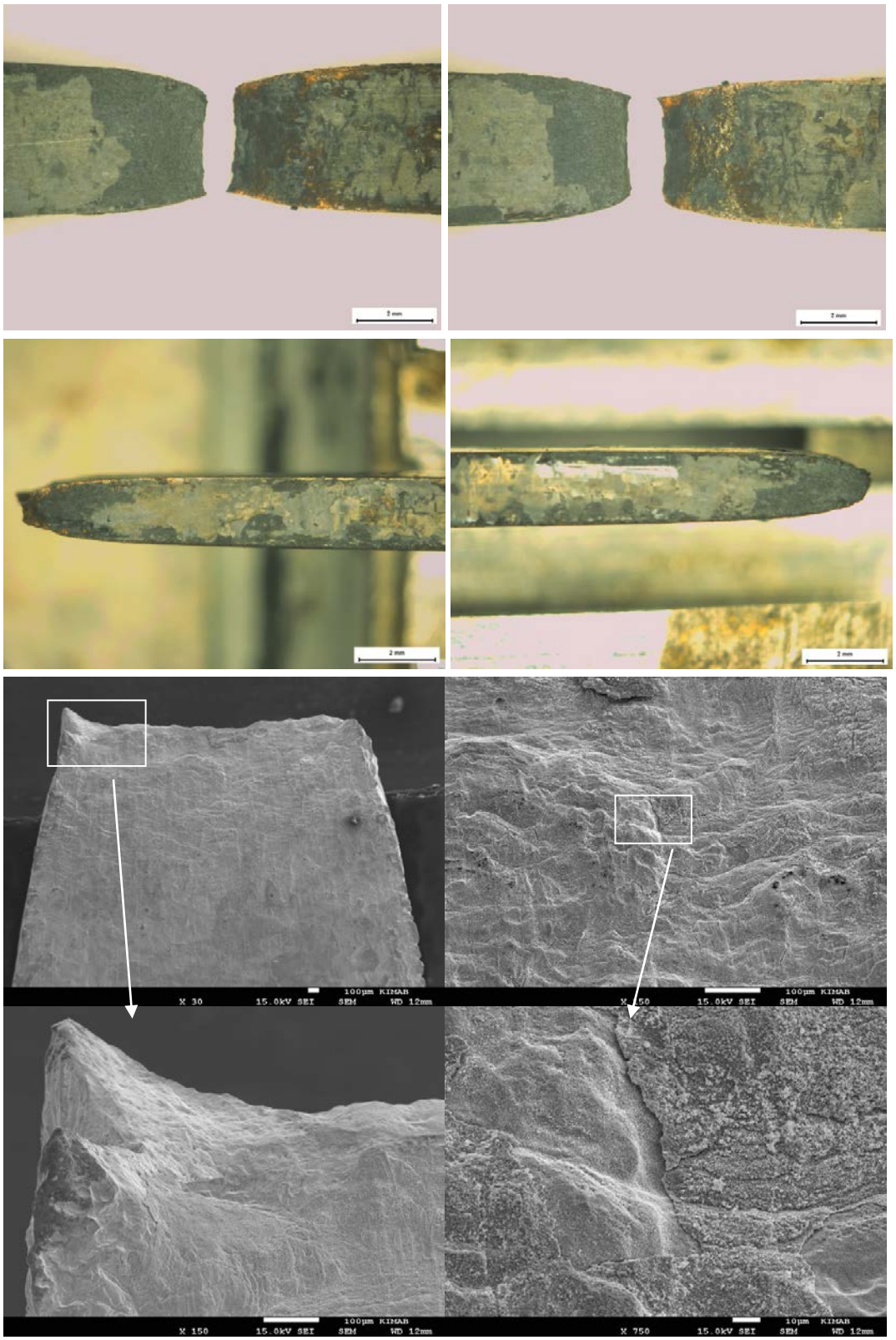


***Figure 3-15.*** *An assembly of images of the test rod for test 7 in synthetic seawater with 10 mM sulfide at 80 °C.*

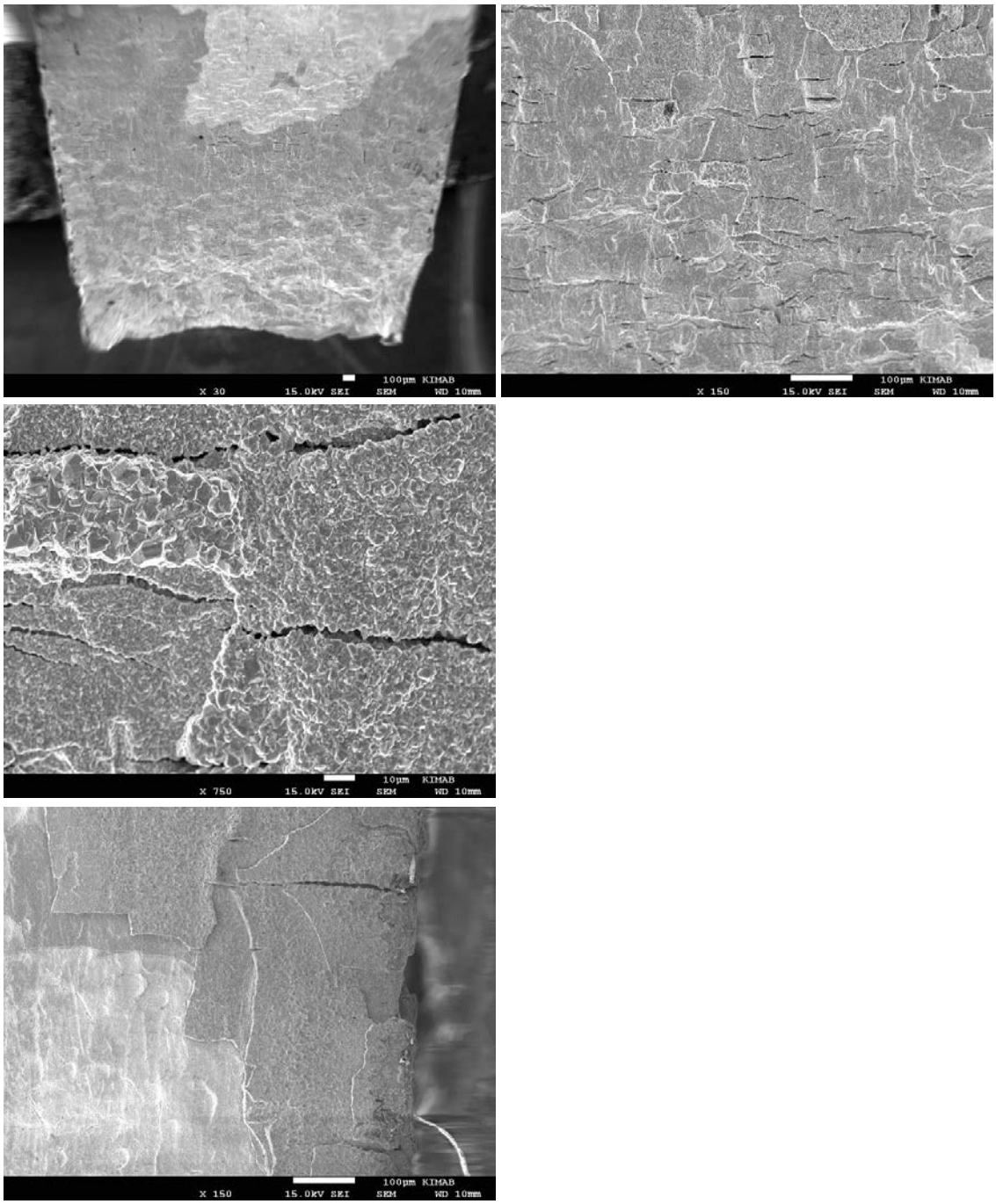


***Figure 3-16.*** *An assembly of images of the test rod for test 9 in synthetic seawater with 10 mM sulfide at 80 °C.*

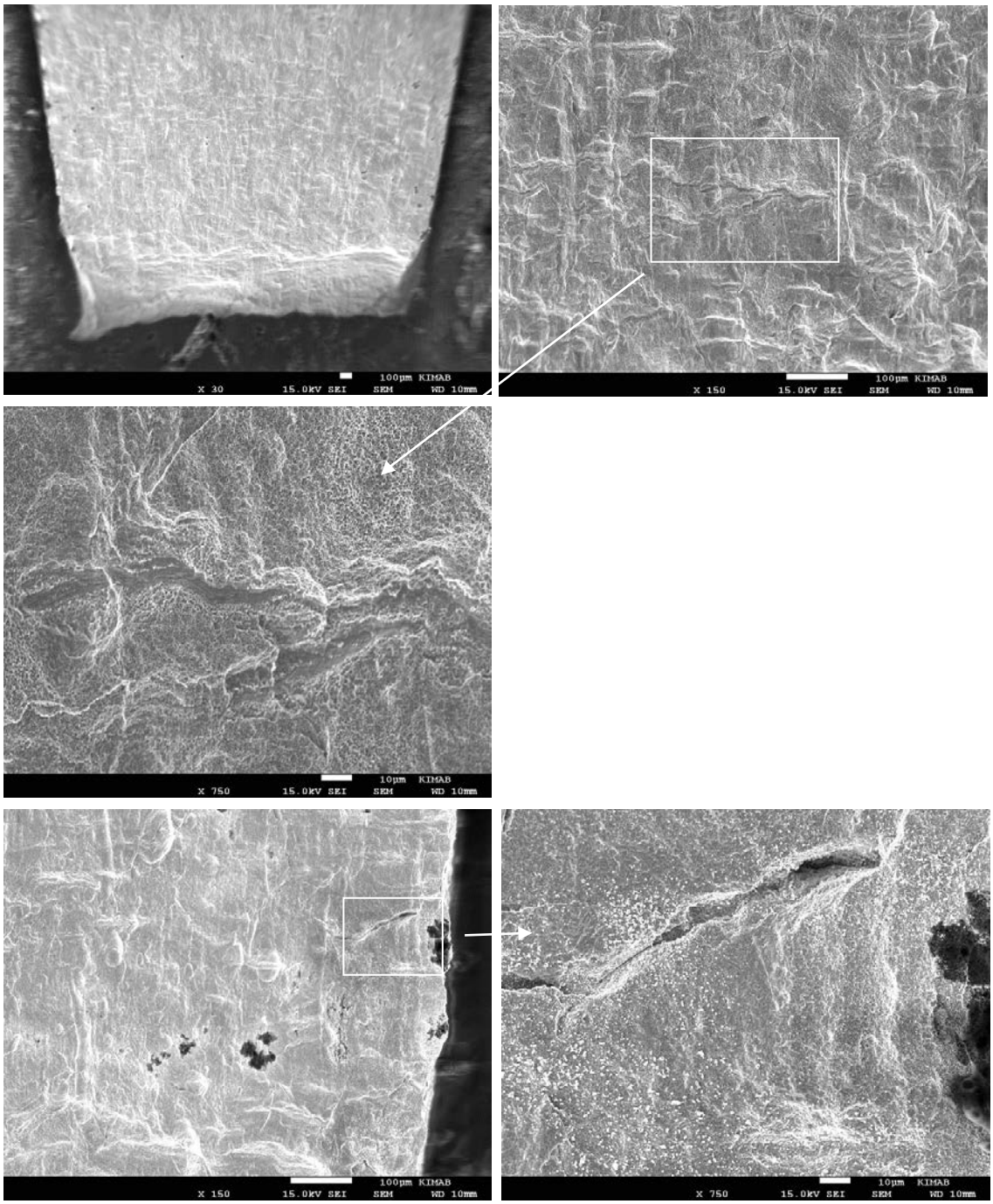


***Figure 3-17.*** *An assembly of images of the test rod for test 9 in synthetic seawater with 10 mM sulfide at 80 °C, after cleaning with HCl.*

# 4 Discussion

Stress-strain curves do not reveal any tendency for SCC in any of the tests. Taniguchi and Kawasaki (2008) report a slightly lower strain at rupture in 0.01 M sulfide than at lower concentrations and seem to interpret this difference as being a sign of SCC. The strain at rupture for lower sulfide concentrations were actually higher than for the reference test in silicone oil, so the differences may be a normal fluctuation in results and may not, by itself, signify a trend.

Bhaskaran et al. (2013) similarly report a slightly lower strain at rupture in 0.01 M sulfide than in air but do not attribute this observation to SCC. The present study shows consistently higher strains at rupture, for the test rods with circular cross section, than Taniguchi and Kawasaki (2008) and Bhaskaran et al. (2013), found for similar conditions. The high values for the strain at rupture observed in the present study may have been influenced by yielding in the SSRT machine.

Becker and Öijerholm (2017) did not pull the test rods to fracture but their stress-strain curves seem almost identical independent of the sulfide concentration. The present work shows almost consistently slightly lower strains at rupture in 0.01 M sulfide than without sulfide. The difference is however very small. The higher general corrosion in sulfide solutions may be one explanation. Decreased cross section of the test rod, by general corrosion, would then cause a higher true stress in the experiments with sulfide than in the experiments without sulfide.

The indications of SCC come from studies of the sides of the test rods close to the fracture and not from the fracture surfaces themselves. Fracture surfaces in the present study generally show only the typical dimpled appearance usually associated with ductile fracture (Figure 3-14). Taniguchi and Kawasaki report many intergranular cracks in the surface close to the fracture. Becker and Öijerholm report some cracks that may or may not be initial defects that have grown wider with the strain. They report also a pattern of surface cracks that seem to follow grain boundaries. Bhaskaran et al. report zig-zag patterns in the surface which they interpret as probably due to enhanced corrosion at sites of film fracture. However, the zig-zag pattern in Figure 1-10 could be seen as being similar to the pattern shown in the right hand corner of Figure 1-3 from the work of Taniguchi and Kawasaki.

The peculiar features at the crack in Figure 3-12 do not signify SCC. Very similar appearance has been observed for specimen strained to fracture in air. Figure 4-1 shows a cross section of the fracture zone of a test rod strained to fracture in air (Björkblad and Faleskog 2017). The white arrows show features where similar appearance was found in the present study for a test in sulfide solution (see Figure 3-12). Thus these features depicted in Figure 3-12 are not related to SCC.

The present study reveals a pattern of corrosion that seems to follow grain boundaries (Figure 3-13). The pattern is evident where the sulfide layer has cracked so that the bare copper surface is exposed. The corrosion grooves seem to follow the crystal structure and not the structure of the corrosion products so the pattern seems closer to the features reported as cracks by Becker and Öijerholm than to the zig-zag patterns reported by Bhaskaran et al. Bhaskaran et al. also report a pattern of corrosion that seemed to follow grain boundaries but since the dimensions of that pattern was much coarser than the microstructure, it seems that the pattern, in that particular case, was due to cracking of the layer of corrosion products.

Preliminary work at VTT used copper test coupons with a pre-crack induced by fatigue. The final cracking after SCC-test was also induced by fatigue. Examination of the material afterwards showed the presence of sulfide in the material some 0.3 mm below the fracture surface. This was, at first, taken as an indication of sulfide/sulfur being able to diffuse from the test solution into the CuOFP grain boundaries which could cause SCC or other types of brittle failure (Sipilä et al. 2014). It is now suggested that the high sulfur contents found in the preliminary work may have been caused by the method of opening op the fracture surfaces (i.e. post-exposure fatigue in air) and that the in-diffusion of sulfide does not take place with such large scale as previously reported, if at all (Sipilä et al. 2014).

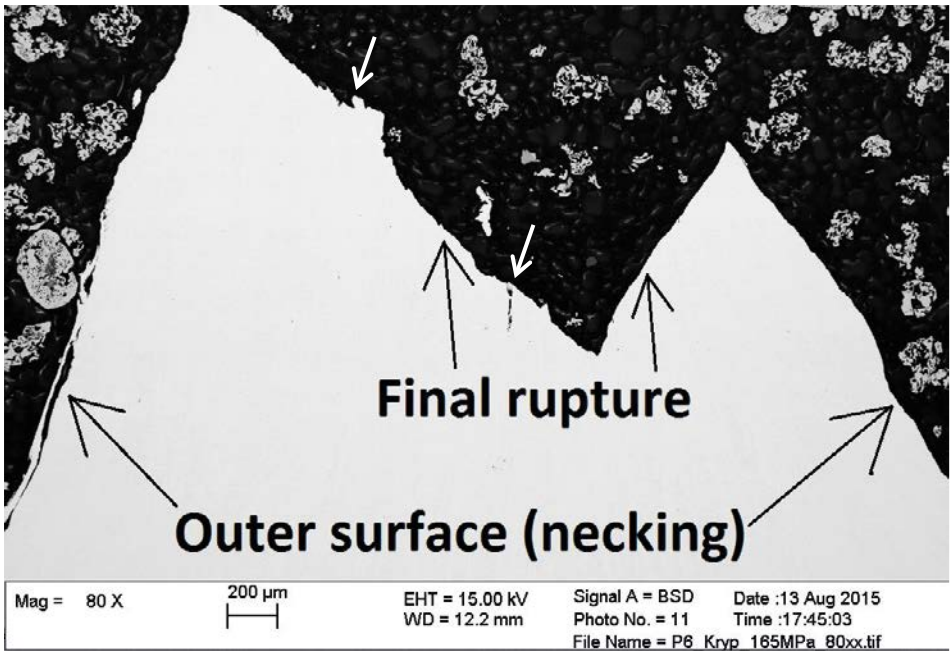


***Figure 4-1.*** *Copper test rod after a creep test in air (Björkblad and Faleskog 2017).*

In later studies only small concentrations or no sulfur at all was found on fracture surfaces. The tests indicated that CuOFP is not susceptible to SCC when exposed to a water with 200 mg/l sulfide at room temperature (Sipilä et al. 2014).

The relatively clear evidence of SCC at 80 °C found by Taniguchi and Kawasaki (2008) has not been reproduced, neither by Bhaskaran et al. (2013) nor by the present study. A possible explanation is the material used. Although the composition is similar there are minor differences.

Becker and Öijerholm (2017) used a material very similar to the material in the present study. However, they performed the study at 90 °C and the increase from 80 °C may be a factor in explaining the apparent shift from superficial grain boundary corrosion found in the present study to the pattern cracks found by Becker and Öijerholm. Other factors are the time of exposure and the strain rate. A rate of $10^{-6}$ $s^{-1}$ was used in the present study whereas Becker and Öijerholm used about $0.7 \times 10^{-7}$ $s^{-1}$ giving an experiment time of 2 weeks. Particularly for the not fully annealed specimens in tests 6, 7 and 8, 9 the time in sulfide solution was significantly shorter than in the work by Becker and Öijerholm. Bhaskaran et al. varied the strain rate down to $10^{-7}$ $s^{-1}$ but always used a preload of 70–108 MPa to shorten the duration of the experiment.

The experimental conditions in the studies are summarised in Table 4-1.

**Table 4-1. Experimental conditions in the studies.**

| | Taniguchi and Kawasaki | Bhaskaran et al. | Becker and Öijerholm | This work |
|---|---|---|---|---|
| Strain rate ($s^{-1}$) | $8.3 \times 10^{-7}$ | $10^{-6}$ or $10^{-7}$ | $0.7 \times 10^{-7}$ | $10^{-6}$ |
| Preload (MPa) | ≈50 | 70–108 | None | None |
| Sulfide conc (mM) | 1, 5, 10 | 5–50 | 0.01, 0.1, 1 | 10 |
| Solution renewal | Periodic | Periodic | Constant flow | Constant flow |
| Base solution | Artificial seawater | Artificial seawater | 0.1 M NaCl + $PO_4$-buffer | Artificial seawater |
| Temperature (°C) | 80 | 80 | 90 | 80 |
| Copper material | See Table 2-1 | SKB-copper | SKB lid TX214 | SKB lid TX219 |
| Time under strain (days, estimated) | <8* | <7** | ≈15 | <8 |

* Based on a strain rate of $8.33 \times 10^{-7}$ $s^{-1}$ and a strain at fracture of 55 %.

** Based on a strain rate of $10^{-6}$ $s^{-1}$ and a strain at fracture of about 55 %. Bhaskaran el at also exposed U-bends for up to 259 hours but apparently only at room temperature.

Note: Only Becker and Öijerholm used a pH buffer.

We can try to identify damaging factor for SCC if we tentatively rank the indications of SCC after a subjective estimate of the strength of the indications.

Taniguchi and Kawasaki are considered to have found the strongest indications for SCC, based on Figures 1-3 and 1-4 and the quoted text after the figures. Becker and Öijerholm can be considered to have found some evidence based mainly on the pattern of cracks or grain boundary corrosion in Figures 1-16 and 1-17. The present study reveals some signs of grain boundary corrosion in Figure 3-13. Bhaskaran et al. found some evidence of superficial intergranular corrosion as shown in Figure 1-12. Based on this ranking of the strength of the evidence, damaging factors for SCC could be:

*The copper material*. Taniguchi and Kawasaki used a copper material which in this context may be seen as having deviant composition. SKB was the supplier of copper to the other three studies. The hardness of the material resulting from cold work may have varied between the test pieces used by the various investigators. However, the present work covers a wide range of hardness of the copper material tested, from fully annealed to severely cold worked copper. No tendency in the sensitivity to SCC, that could be attributed to variations in hardness, can be seen in the results.

*Strain rate* which is tightly connected to the time of exposure under strain. Becker and Öijerholm used the lowest strain rate giving the longest duration of exposure under strain.

*The pH of the test solution.* Becker and Öijerholm used a pH buffer to maintain neutral pH. The other studies did, in general, not control the pH.

*Temperature.* Becker and Öijerholm used the highest temperature and produced indications of SCC in spite of the low sulfide concentrations used.

High concentrations of sulfide do not appear as a particularly damaging factor in this assessment.

Thus also for high purity copper the minor alloying elements or impurities may play a role for the sensitivity to SCC in sulfide solutions. Longer time in the sulfide solutions (coupled to low strain rates) give more pronounced corrosion effects. A higher temperature could be damaging because most processes proceed with higher rate at increased temperature.

A detrimental effect of neutral pH relative to alkaline pH coupled to a relatively low sensitivity to the concentration of sulfide could indicate that a particular chemical specie promotes SCC. If $H_2S$ would promote SCC but not $HS^-$, a decrease in the pH-value from say pH 10 to pH 9 would have the same effect as increasing the sulfide concentration from 1 mM to 10 mM at pH 10. The possibility that SCC was caused by other species than $HS^-$ was studied by Bhaskaran et al. who added also thiosulfate to the test solution but found no effect on the tendency to SCC.

# 5 Conclusions

Two types of test rods were tested by SSRT at room temperature and at 80 °C. The test solution was artificial sea water with 10 mM sulfide. The stress-strain diagrams, the metallic surfaces beneath the corrosion products and the fracture zones were examined for signs of stress corrosion cracking. Comparisons were made with tests without sulfide.

Based on the experimental evidence we find no clear evidence of SCC. However we do find some features from metallographic examination of the specimens that are similar to observations by other investigators and by them taken as indications of SCC.

The strongest evidence of corrosion that could lead to stress corrosion cracking, in presence of 10 mM sulfide in the long run, found in the present study was a pattern of what seems to be superficial grain boundary attack.

# References

SKB's (Svensk Kärnbränslehantering AB) publications can be found at www.skb.com/publications. SKBdoc documents will be submitted upon request to document@skb.se.


**Björkblad A, Faleskog J, 2017.** Evaluation of Cu-OFP creep crack growth and theoretical fracture models for Cu-OFP. Posiva SKB Report 03, Posiva Oy, Svensk Kärnbränslehantering AB.

**Becker R, Öijerholm J, 2017.** Slow strain rate testing of copper in sulfide rich chloride containing deoxygenated water at 90 °C. SSM report 2017:02. Swedish Radiation Safety Authority.

**Bhaskaran G, Carcea A, Ulaganathan J, Wang S, Huang Y, Newman R C, 2013.** Fundamental aspects of stress corrosion cracking of copper relevant to the Swedish deep geologic repository concept. SKB TR-12-06, Svensk Kärnbränslehantering AB.

**Farina S B, Duffó G S, Galvele J R, 2005.** Stress corrosion cracking of copper and silver, specific effect of the metal cations. Corrosion Science 47, 239–245

**Jonsson M, Ronneteg U, 2014.** Manufacturing and testing of copper compounds. SKBdoc 1432038 ver 1.0, Svensk Kärnbränslehantering AB.

**King F, Newman R, 2010.** Stress corrosion cracking of copper canisters. SKB TR-10-04, Svensk Kärnbränslehantering AB.

**Kužnicka B, Junik K, 2007.** Intergranular stress corrosion cracking of copper – A case study. Corrosion Science 49, 3905–3916

**Sipilä K, Arilahti E, Lehtikuusi T, Saario T, 2014.** Effect of sulfide exposure on mechanical properties of CuOFP. Corrosion Engineering, Science and Technology 49, 410–414.

**SKB, 2010.** Fuel and canister process report for the safety assessment SR-Site. SKB TR-10-46, Svensk Kärnbränslehantering AB.

**Taniguchi N, Kawasaki M, 2008.** Influence of sulfide concentration on the corrosion behavior of pure copper in synthetic seawater. Journal of Nuclear Materials 379, 154–161.

Arkitektkopia AB, Bromma, 2018

SKB is responsible for managing spent nuclear fuel and radioactive waste produced by the Swedish nuclear power plants such that man and the environment are protected in the near and distant future.

**skb.se**